$[\beta\text{-}Na_2Fe_{18}S_{30}]^{8-}$ and $[Na_9Fe_{20}Se_{38}]^{9-}$: High-Nuclearity Clusters by Mono- or Bicyclization of Unidimensional Polymeric Fragments and the Existence of Isomeric Monocyclic Clusters

Jing-Feng You,[†] G. C. Papaefthymiou,[‡] and R. H. Holm*,[†]

Contribution from the Department of Chemistry, Harvard University, Cambridge, Massachusetts 02138, and the Francis Bitter National Magnet Laboratory, Massachusetts Institute of Technology, Cambridge, Massachusetts 02139. *Received August 19, 1991*

Abstract: Alteration of conditions in the assembly system that has previously afforded the cyclic cluster $[\alpha\text{-}Na_2Fe_{18}S_{30}]^{8-}$ has led to the preparation of two new high-nuclearity clusters of unprecedented structure. The system $FeCl_3$:3Na(PhNCOMe):nLi_2Q/EtOH (n = 1.8 for Q = S; n = 2 for Q = Se), when treated with Bu_4NBr after 10–12 h and allowed to react and crystallize over 5 days, affords the black compounds $(Bu_4N)_6Na_4Fe_{18}S_{30}$ (**1**) or $(Bu_4N)_{4.5}Na_{13.5}Fe_{20}Se_{38}$·2PhNHCOMe·12EtOH (**2**·12EtOH) in good yield. Compound **1**·8EtOH (**2**·15EtOH) crystallizes in monoclinic (orthorhombic) space group $P2_1/n$ ($Pbcn$) with a = 17.862 (5) (34.551 (11)) Å, b = 27.383 (11) (26.169 (5)) Å, c = 18.534 (6) (24.244 (8)) Å, β = 91.12 (2)°, and Z = 2 (4). The crystal structures include discrete Bu_4N^+ ions, solvate molecules (EtOH, PhNHCOMe), and cluster anions. Compound **1**·8EtOH contains the *monocyclic* cluster $[\beta\text{-}Na_2Fe_{18}S_{30}]^{8-}$, which has a centrosymmetric toroidal shape of lateral dimensions 12.4 × 16.3 Å, a maximum thickness of 3.3 Å, and no terminal ligands. It is constructed by the fusion of 22 nonplanar Fe_2S_2 rhombs in edge- and vertex-sharing modes such that there are 18 μ_2-S and 12 μ_3-S atoms binding 18 nearly coplanar iron atoms in tetrahedral FeS_4 sites. Two sodium ions are bound to interior sulfur atoms of the cluster whose framework can be considered to arise from the sequential connection of two Fe_2S_2 and four cuboidal Fe_3S_4 fragments and two tetrahedral FeS_4 sites. This cluster is a *structural isomer* of $[\alpha\text{-}Na_2Fe_{18}S_{30}]^{8-}$ whose atom connectivity is different (20 μ_2-S, 8 μ_3-S, 2 μ_4-S, 2 Fe_3S_4 + 2 Fe_6S_9 fragments). A structural comparison of the two isomers is presented. Compound **2**·12EtOH contains the *bicyclic* cluster $[Na_9Fe_{20}Se_{38}]^{9-}$ of prolate ellipsoidal shape with the dimensions 11.2 × 17.4 Å, imposed C_2 symmetry, and no terminal ligands. The structure is built up from 21 nonplanar Fe_2Se_2 rhombs, 15 of which share vertices to form three separate but equivalent $Fe_6(\mu_2\text{-}Se)_{10}$ chains. These chains, positioned roughly parallel to an idealized C_3 axis that contains the additional two nonchain Fe atoms and two Se atoms, are anchored at each end of the molecule by attachment to three edge-shared bridgehead rhombs. Nine sodium ions are encapsulated within the selenium-rich interior cavity, distinguishing the molecule as inorganic thiacryptand. $[Na_9Fe_{20}Se_{38}]^{9-}$ is the only known bicyclic cluster. Both clusters have singlet ground states, are electronically delocalized and antiferromagnetically coupled, and are of dimensions that place them in the nanometer size range. Magnetic and Mössbauer spectroscopic data are reported. Reaction of $[Na_9Fe_{20}Se_{38}]^{9-}$ with p-toluenethiol causes breakdown to the major product $[Fe_4Se_4(S\text{-}p\text{-}tol)_4]^{2-}$ and minor amounts of $[Fe_6Se_9(S\text{-}p\text{-}tol)_2]^{4-}$ and $[Fe_2Se_2(S\text{-}p\text{-}tol)_4]^{2-}$. The electronic structures of the two clusters as analyzed at the extended Hückel level have quasiband structures in which the highly delocalized MO's divide into five distinct blocks. Leading results from this analysis are described. It is suggested that clusters $[\alpha\text{-}Na_2Fe_{18}S_{30}]^{8-}$, $[\beta\text{-}Na_2Fe_{18}S_{30}]^{8-}$, and $[Na_9Fe_{20}Se_{38}]^{9-}$ can be assembled from a common cyclic precursor $[Fe^{III}{}_{14}Q_{28}]^{14-}$ and that the α- and β-isomers of the cyclic cluster can be interconverted by relatively minor bond rearrangements. The existence of these isomers is predicted from molecular topological arguments, which are briefly summarized. The general concept demonstrated by these clusters is that, under promotion by an appropriate reagent, high-nuclearity clusters can be formed by termination of unidimensional polymeric fragments via mono- or bicyclization.

Introduction

The chemistry of metal cluster molecules with dimensions in the nanometer size range is attracting increased attention in the exploration of the largely uncharted area between conventional molecular solids and infinite atomic arrays of solid-state compounds.[1-5] In the area of metal chalcogenides, high-nuclearity molecular clusters have been assembled, stabilized, and solubilized most effectively by the use of tertiary phosphines as terminal ligands. Striking examples include $Ni_{20}Te_{18}(PEt_3)_{12}$,[6] $Pd_{20}As_{12}(PPh_3)_{12}$,[7] $Ni_{34}Se_{22}(PPh_3)_{10}$,[8] $Cu_{36}Se_{18}(PtBu_3)_{12}$,[9] and $Cu_{70}Se_{35}(PEt_3)_{22}$.[10]

In our studies of iron–sulfur clusters, we have observed that all known structures can be conceived as systematically built up by vertex- and/or edge-sharing of Fe_2S_2 rhombs.[11] These sharing modes, alone or in combination, are found in the clusters of known structures with nuclearities 2–4, 6–8, 18, and 20.[12,13] Structural complexity nearly culminates with $[Na_2Fe_{18}S_{30}]^{8-}$, a *cyclic* cluster whose structure is depicted in Figure 1. The cluster is constructed by the fusion of 24 nonplanar rhombs such that there are 20 μ_2-S, 8 μ_3-S, and 2 μ_4-S atoms binding 18 coplanar Fe atoms in tetrahedral sites. This structure, in particular, raises the question of uniqueness, i.e., more than one connectivity pattern of Fe_2S_2 rhombs leading to structural isomers. Such a question can be examined by considerations of molecular topology.

[†] Harvard University.
[‡] Massachusetts Institute of Technology.

(1) Schmid, G. *Struct. Bonding (Berlin)* **1985**, *62*, 51. Schmid, G. *Polyhedron* **1988**, *7*, 2321.
(2) Kharas, K. C. C.; Dahl, L. F. *Adv. Chem. Phys.* **1988**, *70*, 1.
(3) (a) Steigerwald, M. L.; Brus, L. E. *Annu. Rev. Mater. Sci.* **1989**, *19*, 471. (b) Bawendi, M. G.; Steigerwald, M. L.; Brus, L. E. *Annu. Rev. Phys. Chem.* **1990**, *41*, 477.
(4) DiSalvo, F. J. *Science* **1990**, *247*, 690.
(5) (a) Teo, B. K.; Zhang, H. *Polyhedron* **1990**, *9*, 1995. (b) Teo, B. K.; Zhang, H.; Shi, X. *J. Am. Chem. Soc.* **1990**, *112*, 8552 and references therein.
(6) Brennan, M. G.; Siegrist, T.; Stuczynski, S. M.; Steigerwald, M. L. *J. Am. Chem. Soc.* **1989**, *111*, 9240.
(7) Fenske, D.; Fleischer, H.; Persau, C. *Angew. Chem., Int. Ed. Engl.* **1989**, *28*, 1665.
(8) Fenske, D.; Ohmer, J.; Hachgenei, J.; Merzweiler, K. *Angew. Chem., Int. Ed. Engl.* **1988**, *27*, 1277.
(9) Fenske, D.; Krautscheid, H.; Balter, S. *Angew. Chem., Int. Ed. Engl.* **1990**, *29*, 796.
(10) Fenske, D.; Krautscheid, H. *Angew. Chem., Int. Ed. Engl.* **1990**, *29*, 1452.
(11) You, J.-F.; Snyder, B. S.; Papaefthymiou, G. C.; Holm, R. H. *J. Am. Chem. Soc.* **1990**, *112*, 1067.
(12) You, J.-F.; Holm, R. H. *Inorg. Chem.* **1991**, *30*, 1431.
(13) Reynolds, M. S.; Holm, R. H. *Inorg. Chem.* **1988**, *27*, 4494. This article contains structural depictions of all but the Fe_{18}[11] and Fe_{20}[12] clusters.

0002-7863/92/1514-2697$03.00/0

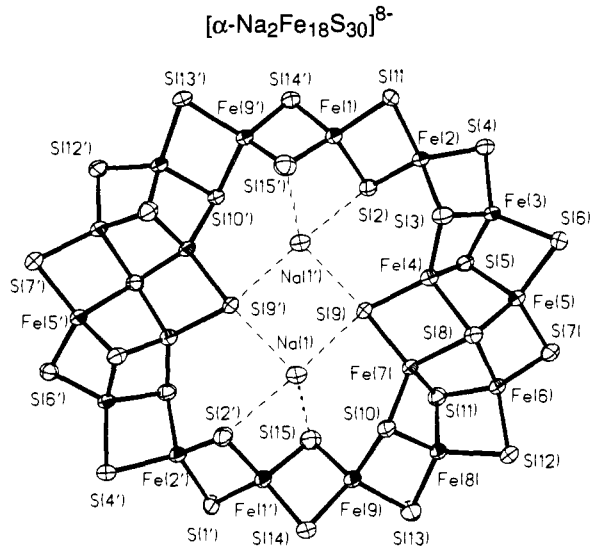

Figure 1. The structure of $[\alpha\text{-}Na_2Fe_{18}S_{30}]^{8-}$ as found in the compound $(Pr_4N)_6Na_4Fe_{18}S_{30}\cdot 14MeCN$.[11]

In metal clusters that are not supported by strong metal–metal interactions, molecular topological closure requires all bonds originating at a metal atom to terminate at either a bridging or terminal ligand atom. Thus for a given formula $[M_mQ_nL_l]^{z-}$, where M is a metal, Q is a μ_2, μ_3, or μ_4 bridging ligand, and L is a terminal ligand, all possible connectivity patterns must meet the topological requirements of eqs 1 and 2, in which n_μ is the number of bridging atoms of a given multiplicity. The number of solutions offered by the two equations is limited, thus allowing specification of all possible bridging mode combinations for a given formula.

$$n = n_{\mu 2} + n_{\mu 3} + n_{\mu 4} \tag{1}$$

$$4m = l + 2n_{\mu 2} + 3n_{\mu 3} + 4n_{\mu 4} \tag{2}$$

For certain formulas, there is only one bridging modality $[n_{\mu 2},n_{\mu 3},n_{\mu 4}]$. Thus, for $[M_3Q_4L_3]^{z-}$ it is [3,1,0] and for $[M_8Q_6L_8]^{z-}$ it is [0,0,6]. However, unique solutions are not usually the case, as illustrated with a tetranuclear cluster. For $[M_4Q_4L_4]^{z-}$, three bridging modalities are possible: [0,4,0], [1,2,1], and [2,0,2]. Each of these is degenerate in the sense that a given modality corresponds to more than one structural isomer. Details of the topological treatment will be developed elsewhere. For the present purpose of illustration, we observe that the modalities accommodate 3 + 3 + 4 = 10 isomers under the limitation that they are constructed entirely from M_2Q_2 rhombs. These isomers (**1–10**) are illustrated in Figure 2.

Among the ten formal isomer possibilities, for M = Fe(II,III) five of these are sterically improbable or impossible because of large distortions from the stereochemically preferred tetrahedral structure of these ions. If we add the further constraint that each iron site has one terminal ligand, a frequent structural feature of Fe–Q clusters, then only two possibilities, **3** and **6**, remain. Both have been realized experimentally, the former as the familiar cubane clusters $[Fe_4Q_4L_4]^{3-,2-,1-}$ (Q = S, Se, Te; L = monoanion). Application of these same constraints to $[Fe_3Q_4L_3]^{z-}$ and $[Fe_8Q_6L_8]^{z-}$ allows only the cuboidal structure, found for protein-bound $Fe_3S_4(S\text{-}Cys)_4$,[14] and the stellated octahedral structure, observed for $[Fe_8S_6I_8]^{3-}$,[15] respectively. In the case of $[M_6Q_6L_6]^{z-}$, there are four bridging modalities: [0,6,0], [1,4,1], [2,2,2], [3,0,3]. The first two of these have been achieved with the prismane clusters $[Fe_6S_6L_6]^{2-,3-}$[16] and the basket clusters $[Fe_6S_6(PR_3)_4L_2]$,[13,17] respectively, which have isomeric (but not isoelectronic) Fe_6S_6 cores.

Application of eqs 1 and 2 to the much more complicated case of $[Fe_{18}S_{30}]^{z-}$ yields seven solutions, emphasizing the possibility of structural isomers. In addition, consideration of the structure

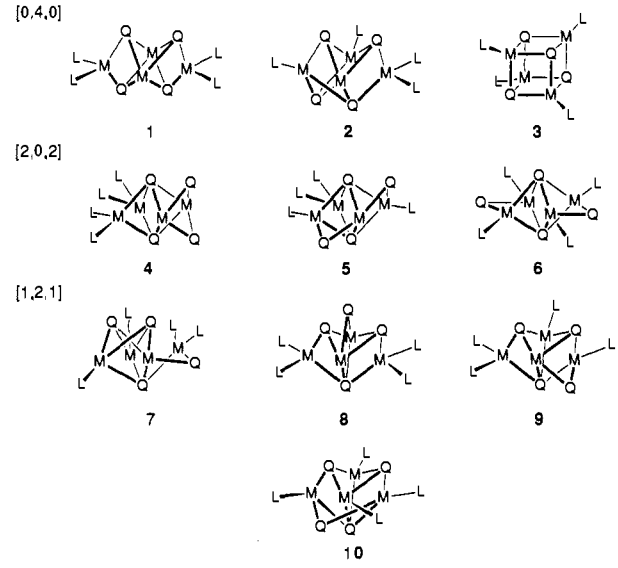

Figure 2. Formulas of the 10 possible structural isomers of the molecule $[M_4Q_4L_4]^{z-}$ built up entirely from M_2Q_2 rhombs. The structures are organized under the bridging modalities $[n_{\mu 2},n_{\mu 3},n_{\mu 4}]$.

of $[Na_2Fe_{18}S_{30}]^{8-}$ raises questions as to the relation of the size of the encapsulated alkali ion and the chalcogenide to the stability of the cyclic configuration. In this virtually unexplored area of large metal–chalcogenide clusters, variation of these size parameters could lead to the synthesis of new cyclic isomers, or to entirely new types of soluble chalcogenoferrates. We have expanded our investigation of cluster self-assembly systems of the type affording $[Na_2Fe_{18}S_{30}]^{8-}$[11] and have successfully prepared an isomer of that cluster, $[\beta\text{-}Na_2Fe_{18}S_{30}]^{8-}$. The structure in Figure 1 is hereafter designated $[\alpha\text{-}Na_2Fe_{18}S_{30}]^{8-}$. Investigation of related assembly systems containing selenide has resulted in the preparation of $[Na_9Fe_{20}Se_{38}]^{9-}$, an unprecedented cluster whose essential structural features we have recently communicated.[12] In this report, we describe full details of the synthesis, structures, and properties of these two new clusters, whose dimensions place them in the nanometer size regime.

Experimental Section

Preparation of Compounds. All operations were carried out under a pure dinitrogen atmosphere. Solvents were thoroughly dried and degassed before use. Li_2Se was prepared by reduction of selenium with $LiEt_3BH$ in THF[18] or with lithium metal in THF.[19]

$(Bu_4N)_6Na_2[\beta\text{-}Na_2Fe_{18}S_{30}]$. The procedure for the preparation of $(Pr_4N)_6Na_2[\alpha\text{-}Na_2Fe_{18}S_{30}]$[11] was followed but with the use of a slurry of 4.41 g (96.0 mmol) of Li_2S in 350 mL of ethanol and 17.4 g (54 mmol) of Bu_4NBr in 50 mL of ethanol. After the product was washed with ethanol and dried, the desolvated cluster compound was obtained as a black crystalline solid in 70–75% yield (multiple preparations). The product was further purified by recrystallization from a solution of 0.15 M Na[PhNC(O)Me] in methanol. The collected solid was washed with 4 × 50 mL of methanol and 2 × 50 mL of ether and dried in vacuo for 10 h. Anal. Calcd for $C_{96}H_{216}Fe_{18}N_6Na_4S_{30}$: C, 32.81; H, 6.20; Fe, 28.61; N, 2.39; Na, 2.62; S, 27.37. Found: C, 32.42; H, 6.21; Fe, 28.36; N, 2.46; Na, 2.99; S, 27.21; Li, 0.0.

Powder X-ray diffraction tests were conducted on bulk samples ob-

(14) (a) Kissinger, C. R.; Adman, E. T.; Sieker, L. C.; Jensen, L. H. *J. Am. Chem. Soc.* **1988**, *110*, 8721. (b) Kissinger, C. R.; Sieker, L. C.; Adman, E. T.; Jensen, L. H. *J. Mol. Biol.* **1991**, *219*, 693. (c) Robbins, A. H.; Stout, C. D. *Proc. Natl. Acad. Sci. U.S.A.* **1989**, *86*, 3639. Robbins, A. H.; Stout, C. D. *Proteins* **1989**, *5*, 289. (d) Stout, C. D. *J. Biol. Chem.* **1988**, *263*, 9256. Stout, C. D. *J. Mol. Biol.* **1989**, *210*, 383.
(15) Pohl, S.; Saak, W. *Angew. Chem., Int. Ed. Engl.* **1984**, *23*, 907.
(16) (a) Kanatzidis, M. G.; Hagen, W. R.; Dunham, W. R.; Lester, R. K.; Coucouvanis, D. *J. Am. Chem. Soc.* **1985**, *107*, 953. (b) Kanatzidis, M.; Salifoglou, A.; Coucouvanis, D. *Inorg. Chem.* **1986**, *25*, 2460.
(17) Snyder, B. S.; Holm, R. H. *Inorg. Chem.* **1988**, *27*, 2339.
(18) Gladysz, J. A.; Hornby, J. L.; Garbe, J. E. *J. Org. Chem.* **1978**, *43*, 1204.
(19) Thompson, D. P.; Bondjouk, P. J. *J. Org. Chem.* **1988**, *53*, 2109.

Table I. Crystallographic Data for $(n\text{-}Bu_4N)_6Na_2[\beta\text{-}Na_2Fe_{18}S_{30}]\cdot 8EtOH$ (**A**) and $(n\text{-}Bu_4N)_{4.5}Na_{4.5}[Na_9Fe_{20}Se_{38}]\cdot 15EtOH\cdot 2MeCONHPh$ (**B**)

	A	B
formula	$C_{112}H_{264}Fe_{18}N_6Na_4O_8S_{30}$	$C_{118}H_{270}Fe_{20}N_{6.5}Na_{13.5}O_{17}Se_{38}$
formula wt	3882.36	6480.25
a, Å	17.862 (5)	34.551 (11)
b, Å	27.383 (11)	26.169 (5)
c, Å	18.534 (6)	24.244 (8)
β, deg	91.12 (2)	
V, Å^3	9063 (6)	21920 (11)
Z	2	4
d_{calcd} (d_{obs}), g/cm^3	1.42[a]	1.96 (1.98)[b]
space group	$P2_1/n$	$Pbcn$
T, K	210	170
μ, cm^{-1}	17.8	70.2
R (R_w), %	9.88 (10.22)	9.93 (9.51)

[a] Accurate density could not be obtained because of solvate composition. [b] Determined in *n*-hexane/dibromomethane.

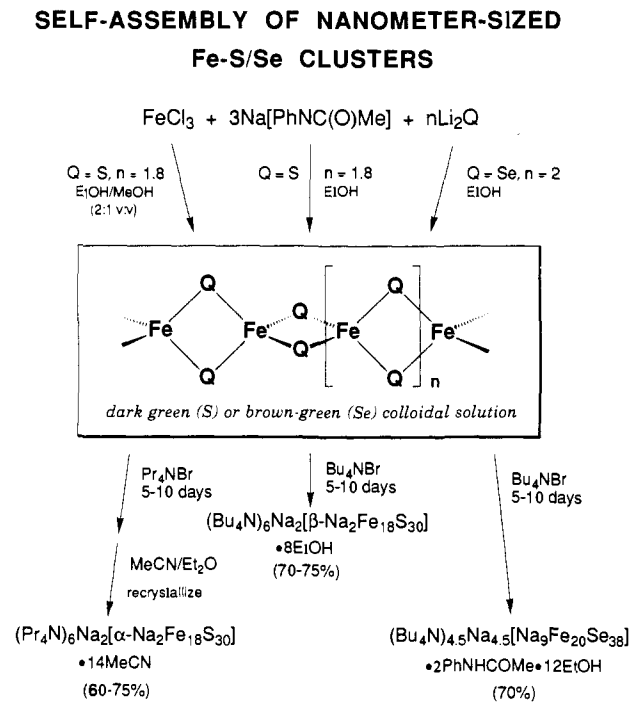

Figure 3. Schematic depiction of the cluster self-assembly systems affording compounds containing $[\alpha\text{-}Na_2Fe_{18}S_{30}]^{8-}$, $[\beta\text{-}Na_2Fe_{18}S_{30}]^{8-}$, and $[Na_9Fe_{20}Se_{38}]^{9-}$. The formulas are those of compounds used in X-ray structural determinations.

tained immediately after the ethanol wash step. These were sealed together with a small amount of ethanol in sample holders with use of X-ray transparent polyimide film. Diffraction patterns were found to agree with the simulated patterns from the single-crystal diffraction data, and there was no evidence of other crystalline phases. The diffraction pattern for this compound is distinctly different from that of $(Pr_4N)_6Na_2[\alpha\text{-}Na_2Fe_{18}S_{30}]\cdot 14MeCN$.[11]

$(Bu_4N)_{4.5}Na_{4.5}[Na_9Fe_{20}Se_{38}]\cdot 2PhNHCOMe\cdot 12EtOH$. A yellow slurry initially containing 3.2 g (20 mmol) of $FeCl_3$ and 60 mmol of Na[PhNC(O)Me] (prepared in situ from the reaction of equimolar quantities of acetanilide and sodium metal) was prepared in 110 mL of ethanol at 5 °C. The mixture was allowed to warm to room temperature with stirring. A clear, off-white solution of 3.72 g (40.0 mmol) of Li_2Se in 110 mL of ethanol was added dropwise with vigorous stirring over 10 h to give a dark brownish-green mixture. The mixture was stirred for an additional 12 h and filtered. A solution of 9.67 g (30.0 mmol) of Bu_4NBr in 30 mL of ethanol was added to the dark brown-green filtrate. A black crystalline product slowly formed over a period of 5–10 days. It was collected by filtration, washed thoroughly with ethanol and ether, and dried in vacuo at room temperature for 10 h. A second crop was obtained by slowly concentrating the filtrate to one-half its original volume and

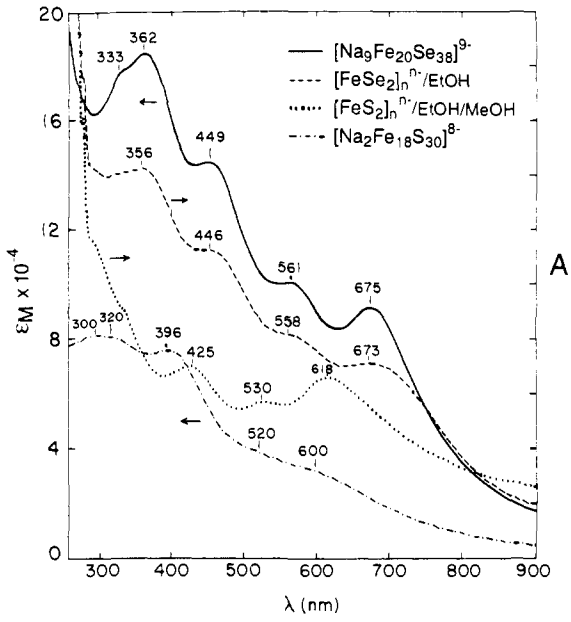

Figure 4. Absorption spectra of $[\beta\text{-}Na_2Fe_{18}S_{30}]^{8-}$ and $[Na_9Fe_{20}Se_{38}]^{9-}$ in acetonitrile, and of their respective precursors $[FeS_2]_n^{n-}$ in EtOH/MeOH (2:1 v/v) and $[FeSe_2]_n^{n-}$ in EtOH. Arrows refer to ϵ_M or absorbance scales; absorption maxima are indicated. Spectra of the α- and β-isomers are indistinguishable.

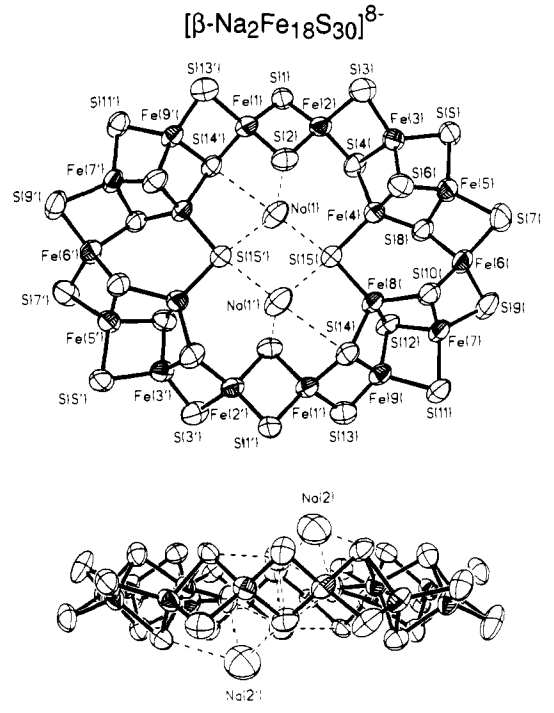

Figure 5. Top and side-on views of the structure of $[\beta\text{-}Na_2Fe_{18}S_{30}]^{8-}$ showing the atom labeling scheme and 50% probability ellipsoids. Atoms Na(1,1') are located within the cluster, and atoms Na(2,2') are positioned above and below the cluster and are weakly bonded to it. Primed and unprimed atoms are related by an imposed inversion center.

carefully layering the solution with 150 mL of 2-propanol. The two crops were combined to afford 4.40 g of product. Analytical results for this material, when compared to the composition deduced from the X-ray structural analysis (Table I), were consistent with an apparent formula for the 12EtOH solvate. Anal. Calcd for $C_{112}H_{252}Fe_{20}N_{6.5}Na_{13.5}O_{14}Se_{38}$: C, 21.21; H, 4.00; Fe, 17.61; N, 1.44; Na, 4.88; Se, 47.31. Found: C, 21.45; H, 4.02; Fe, 17.83; N, 1.68; Na, 4.88; Se, 47.97; Li, 0.0. Calcd Se:Fe atom ratio: 1.90. Found (EDS, chemical analysis): 1.86, 1.88.

X-ray powder diffraction patterns of bulk samples were obtained immediately after washing with ethanol as for compound A. The patterns were found to agree with the simulated powder diffraction pattern from the single-crystal diffraction data, and no line that is not associated with

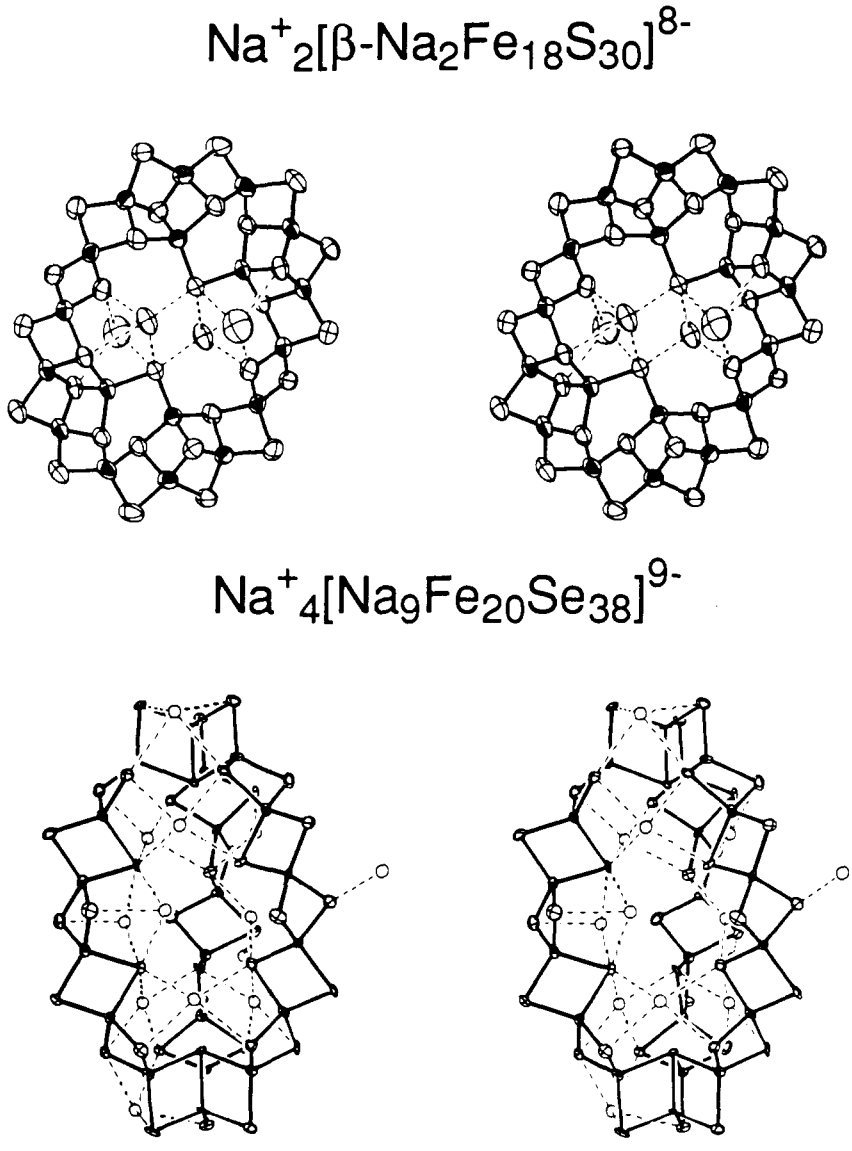

Figure 6. Stereoviews of the structures of $[\beta\text{-}Na_2Fe_{18}S_{30}]^{8-}$ (upper) and $[Na_9Fe_{20}Se_{38}]^{9-}$ (lower); a stereoview of $[\alpha\text{-}Na_2Fe_{18}S_{30}]^{8-}$ is given in ref 11.

the simulated pattern was observed. The absorption spectrum of single crystals isomorphous with that used in the X-ray structural determination was identical with that of the bulk sample. Absorption spectrum (acetonitrile): λ_{max} ($\epsilon_M \times 10^{-3}$) 333 (sh, 178), 362 (185), 449 (145), 561 (101), 675 (94) nm.

Both compounds are freely soluble in acetonitrile, DMF, and Me_2SO and slightly soluble in methanol where they are marginally stable. The compounds are more soluble and stable in Na(PhCOMe)/methanol solutions. In these media, $[\beta\text{-}Na_2Fe_{18}S_{30}]^{8-}$ and $[Na_9Fe_{20}Se_{38}]^{9-}$ form dark brown and brownish-green solutions, respectively.

Collection and Reduction of X-ray Data. Diffraction-quality crystals of compounds A and B, designated in Table I, were obtained by the following procedure. Solid Bu_4NBr was placed at the bottom of a tube with an i.d. of 1.5 cm and a length of 40 cm. Ethanol (10 mL) was added, and reaction mixture filtrate was very slowly layered on top of the ethanol until the tube was nearly full. In both cases, the filtrate was that of the reaction mixture 12 h after Li_2S or Li_2Se (and before any quaternary ammonium cation) had been added. The tubes were allowed to stand at room temperature for periods of one month or more. Black crystals, which formed on the sides of the tube, were removed from the mother liquor and immediately coated with Apiezon grease. Data collections were carried out at low temperatures on a Nicolet P3F diffractometer with use of graphite-monochromatized Mo Kα radiation. Intensities of three check reflections monitored every 100 reflections over the course of the data collections indicated decays of ca. 10%, which were corrected by processing the data sets with the program XDISK of the SHELXTL program package. Empirical absorption corrections were applied with the program DIFABS of the CRYSTALS package. Crystallographic data are contained in Table I.

Crystals of high diffraction quality of compound A were not obtained. Data were collected on a crystal which, as judged by axial photographs and peak profiles, had a small daughter crystal with diffraction intensities less than 10% those of the parent. Unit cell parameters were obtained from 40 machine-centered reflections ($23° \leq 2\theta \leq 25°$). Axial photographs indicated the Laue class $2/m$, and the systematic absences $h0l$ ($h + l = 2n + 1$) and $0k0$ ($k = 2n + 1$) uniquely led to monoclinic space group $P2_1/n$. Unit cell parameters of compound B were obtained from 30 machine-centered reflections ($25° \leq 2\theta \leq 28°$). Axial photographs indicated Laue class $2/mmm$, and the systematic absences $0kl$ ($k = 2n + 1$), $h0l$ ($l = 2n + 1$), and $hk0$ ($h + k = 2n + 1$) are consistent only with orthorhombic space group *Pbcn*. In both cases, simple E statistics also indicated a centrosymmetric space group, and subsequent solutions and refinements of the structures confirmed the assignments.

Structure Solutions and Refinements. Atom scattering factors were taken from a standard source.[20] All iron and sulfur or selenium atoms were located by direct methods using the program R-SAPI. All other non-hydrogen atoms were located in successive difference Fourier maps and were refined using CRYSTALS.

(a) Compound A. Isotropic refinement converged at $R = 12\%$. All iron, sulfur, and sodium atoms and all non-hydrogen atoms of two of the three independent Bu_4N^+ cations were refined anisotropically; all remaining non-hydrogen atoms were described isotropically. Both lengths and distances of Bu_4N^+[21] and ethanol solvate molecules[22] associated with sodium ions were loosely constrained to their normal values with esd's

(20) Cromer, D. T.; Waber, J. T. *International Tables for X-Ray Crystallography*; Kynoch Press: Birmingham, England, 1974.

of 0.03 Å and 1.0°, respectively. In the final stages of refinement, hydrogen atoms were included at 0.95 Å from bonded carbon atoms with the isotropic thermal parameter 8.0 Å^2. A final difference Fourier map revealed several peaks in the 0.3–0.8 e$^-$/Å^3 range that were within bonding distance of certain iron atoms, and are probable artifacts from crystal twinning. The small standard deviations on the positional parameters[23] of the iron and sulfur atoms indicate that the heavy atom portion of the structure is well-defined.

(b) Compound B. Isotropic refinement converged at $R = 11\%$. All iron and selenium atoms were refined anisotropically, and all remaining non-hydrogen atoms isotropically. In the final stages of refinement, bond lengths and distances of Bu_4N^+ and acetanilide[24] and ethanol solvate molecules were constrained and hydrogen atoms included as in the preceding refinement. One special equivalent site of C_2 symmetry was treated by a model based on 1:1 mixed occupancy of Bu_4N^+ and $[Na(EtOH)_4]^+$. In addition, there is one disordered ethanol solvate molecule and a half-interstitial ethanol molecule. These occupancies were fixed at values determined in earlier refinements. As in the previous case, the small standard deviations on the positional parameters of the iron and selenium atoms indicate that the heavy atom portion of the structure is well-defined.

Other Physical Measurements. All measurements were carried out under strictly anaerobic conditions. Magnetic susceptibility and Mössbauer spectroscopic measurements were performed with the equipment described elsewhere,[25] as were absorption spectral, ^{1}H NMR, and electrochemical determinations.[17] Isomer shifts (^{57}Fe) are reported relative to iron metal at room temperature. Electrochemical experiments were performed in DMF solutions with use of a Pt working electrode, a SCE reference electrode, and 0.3 M $Bu_4N(BF_4)$ supporting electrolyte. Powder X-ray diffraction measurements were made with a Rigaku D/Max-2BX Horizontal XRD System.

Results and Discussion

We have recently devised the cluster self-assembly system with initial mol ratio $3FeCl_3$:3Na(PhNCOMe):$3.15Li_2S$.[11] As indicated in Figure 3, the colloidal dark brown-green intermediate first encountered is formulated as the polymeric anion $[FeS_2]_n^{n-}$ whose development is promoted by sodium acetanilate. By controlled crystallization, the intermediate slowly converts to the final product, cyclic $[\alpha\text{-}Na_2Fe_{18}S_{30}]^{8-}$. This cluster now carries the "α" designation for, as will be shown, the structure in Figure 1 is not the only one that can be assumed by a cluster of this composition.

Examination of the structure of $[\alpha\text{-}Na_2Fe_{18}S_{30}]^{8-}$ clearly reveals that the two encapsulated sodium ions, which exhibit four bonding interactions with sulfur atoms, are significant in stabilizing this cluster of high negative charge. Further, these ions may exercise a template effect inducing the formation of the cyclic structure. These thoughts are supported by a space-filling modeling study and by extended Hückel calculations.[11] Indeed, when Na^+ was replaced with Li^+ in the synthesis the reaction stopped at the dark green intermediate stage, and the absorption spectrum of the mixture remained unchanged for 2 weeks from that of $[FeS_2]_n^{n-}$, which is shown in Figure 4. The use of K^+ resulted in formation of a dark green intractable solid (probably $KFeS_2$) and a colorless supernatant. In addition to the critical role of Na^+, the choice of the precipitating cation R_4N^+ is essential to cluster formation. With Et_4N^+, insoluble $Et_4N(FeS_2)$ was obtained as a dark green solid; without Pr_4N^+, the reaction system remained as a dark green mixture and did not achieve significant cluster formation. These findings emphasize the specific requirements of the assembly system and imply that it might be redirected to other cluster products upon change of reaction conditions or of chalcogenide. This possibility, abetted by the foregoing topological considerations, encouraged further investigation of the related cluster assembly systems summarized in Figure 3, resulting in the synthesis of two new clusters with unanticipated structures.

Table II. Selected Interatomic Distances (Å) for $[\beta\text{-}Na_2Fe_{18}S_{30}]^{8-}$

	Fe···Fe		
Fe(1)–Fe(2)	2.717 (3)	Fe(1)–Fe(9′)	2.751 (3)
Fe(2)–Fe(3)	2.723 (3)	Fe(3)–Fe(4)	2.763 (3)
Fe(3)–Fe(5)	2.678 (3)	Fe(4)–Fe(5)	2.771 (3)
Fe(5)–Fe(6)	2.689 (4)	Fe(6)–Fe(7)	2.697 (3)
Fe(7)–Fe(8)	2.740 (3)	Fe(7)–Fe(9)	2.698 (3)
Fe(8)–Fe(9)	2.742 (3)		
mean of 11	2.72 (3)		
	Fe–(μ_2-S)		
Fe(1)–S(1)	2.227 (5)	Fe(1)–S(2)	2.209 (5)
Fe(1)–S(13′)	2.236 (6)	Fe(2)–S(1)	2.191 (5)
Fe(2)–S(2)	2.230 (5)	Fe(2)–S(3)	2.218 (5)
Fe(3)–S(3)	2.178 (6)	Fe(3)–S(5)	2.213 (5)
Fe(4)–S(15)	2.262 (5)	Fe(5)–S(5)	2.200 (5)
Fe(5)–S(7)	2.205 (5)	Fe(6)–S(7)	2.197 (6)
Fe(6)–S(9)	2.206 (6)	Fe(7)–S(9)	2.228 (5)
Fe(7)–S(11)	2.214 (5)	Fe(8)–S(15)	2.264 (5)
Fe(9)–S(11)	2.224 (5)	Fe(9)–S(13)	2.180 (6)
mean of 18	2.22 (2)		
	Fe–(μ_3-S)		
Fe(1)–S(14′)	2.291 (5)	Fe(2)–S(4)	2.303 (5)
Fe(3)–S(4)	2.315 (5)	Fe(3)–S(6)	2.285 (5)
Fe(4)–S(4)	2.327 (5)	Fe(4)–S(6)	2.287 (5)
Fe(5)–S(6)	2.320 (5)	Fe(4)–S(8)	2.315 (5)
Fe(5)–S(8)	2.317 (6)	Fe(6)–S(8)	2.260 (5)
Fe(6)–S(10)	2.332 (5)	Fe(7)–S(10)	2.267 (5)
Fe(7)–S(12)	2.284 (5)	Fe(8)–S(10)	2.275 (5)
Fe(8)–S(12)	2.264 (5)	Fe(8)–S(14)	2.352 (4)
Fe(9)–S(12)	2.296 (4)	Fe(9)–S(14)	2.330 (5)
mean of 18	2.30 (3)		
	Na···S		
Na(1)–S(2)	2.96 (1)	Na(2)–S(2)	2.89 (1)
Na(1)–S(15)	2.847 (8)	Na(2)–S(12′)	3.19 (1)
Na(1)–S(15′)	2.984 (8)	Na(2)–S(15)	3.04 (1)
Na(1)–S(14′)	3.049 (8)		
Na(1)–S(4)	3.578 (9)		
	Na···O(HOEt)		
Na(1)–O(1)	2.24 (2)	Na(1)–O(2)	2.60 (2)
Na(2)–O(2)	2.37 (2)	Na(2)–O(3)	2.26 (2)
Na(2)–O(4)	2.39 (2)		
	S···S		
S(1)–S(2)	3.496 (6)	S(1)–S(3)	3.721 (7)
S(1)–S(4)	3.732 (6)	S(1)–S(13′)	3.759 (7)
S(1)–S(14′)	3.754 (6)	S(2)–S(3)	3.727 (7)
S(2)–S(4)	3.690 (7)	S(2)–S(13′)	3.739 (7)
S(2)–S(14′)	3.633 (6)	S(2)–S(15)	4.041 (6)
S(3)–S(4)	3.522 (7)	S(3)–S(5)	3.803 (8)
S(3)–S(6)	3.730 (6)	S(4)–S(5)	3.771 (6)
S(4)–S(6)	3.636 (6)	S(4)–S(8)	3.596 (6)
S(4)–S(15)	3.863 (6)	S(5)–S(6)	3.504 (6)
S(5)–S(7)	3.801 (6)	S(5)–S(8)	3.792 (7)
S(6)–S(7)	3.853 (7)	S(6)–S(8)	3.643 (7)
S(6)–S(10)	3.945 (6)	S(6)–S(15)	3.838 (7)
S(7)–S(8)	3.490 (7)	S(7)–S(9)	3.791 (9)
S(7)–S(10)	3.752 (6)	S(8)–S(9)	3.722 (6)
S(8)–S(10)	3.731 (6)	S(8)–S(12)	3.860 (6)
S(8)–S(15)	3.867 (6)	S(9)–S(10)	3.515 (7)
S(9)–S(11)	3.858 (7)	S(9)–S(12)	3.783 (7)
S(10)–S(11)	3.754 (7)	S(10)–S(12)	3.583 (7)
S(10)–S(14)	3.552 (6)	S(10)–S(15)	3.958 (6)
S(11)–S(12)	3.468 (6)	S(11)–S(13)	3.786 (7)
S(11)–S(14)	3.825 (6)	S(12)–S(13)	3.759 (6)
S(12)–S(14)	3.674 (6)	S(12)–S(15)	3.742 (6)
S(13)–S(14)	3.555 (7)	S(14)–S(15)	3.837 (6)
S(15)–S(15′)	4.076 (8)		
S(1)–S(1′)	12.39	S(9)–S(9′)	16.29
	Na···Na		
Na(1)–Na(1′)	4.17 (1)	Na(1)–Na(2)	3.82 (1)
Na(1)–Na(2′)	4.16 (1)		

$[\beta\text{-}Na_2Fe_{18}S_{30}]^{8-}$. (a) Cluster Synthesis. The cluster assembly reaction system is set out in Figure 3. Following a procedure very

(21) Dahlstrom, P.; Zubieta, J.; Neaves, B.; Dilworth, J. R. *Cryst. Struct. Commun.* **1982**, *11*, 463.

(22) (a) Hughes, D. L.; Wingfield, J. N. *J. Chem. Soc., Chem. Commun.* **1984**, 408. (b) Sachleben, R. A.; Burns, J. H.; Brown, G. M. *Inorg. Chem.* **1988**, *27*, 1787.

(23) See the paragraph at the end of this article concerning supplementary material available.

(24) (a) Brown, C. J. *Acta Crystallogr.* **1966**, *21*, 442. (b) Wasserman, H. J.; Ryan, R. R.; Layne, S. P. *Acta Crystallogr.* **1985**, *C41*, 783.

(25) Carney, M. J.; Papaefthymiou, G. C.; Whitener, M. A.; Spartalian, K.; Frankel, R. B.; Holm, R. H. *Inorg. Chem.* **1988**, *27*, 346.

Table III. Selected Angles (deg) for $[\beta\text{-}Na_2Fe_{18}S_{30}]^{8-}$

		Fe···Fe···Fe	
		In the Ring Perimeter	
Fe(9′)–Fe(1)–Fe(2)	168.9 (1)	Fe(3)–Fe(2)–Fe(1)	163.3 (1)
Fe(6)–Fe(5)–Fe(3)	145.8 (1)	Fe(5)–Fe(3)–Fe(2)	147.5 (1)
Fe(7)–Fe(6)–Fe(5)	149.0 (1)	Fe(9)–Fe(7)–Fe(6)	144.3 (1)
Fe(7)–Fe(9)–Fe(1′)	150.4 (1)		
		In the Fe_3S_4 Units	
Fe(5)–Fe(3)–Fe(4)	61.20 (9)	Fe(5)–Fe(4)–Fe(3)	57.88 (8)
Fe(4)–Fe(5)–Fe(3)	60.92 (8)	Fe(9)–Fe(8)–Fe(7)	58.98 (8)
Fe(9)–Fe(7)–Fe(8)	60.55 (8)	Fe(8)–Fe(9)–Fe(7)	60.47 (8)
		Elsewhere	
Fe(4)–Fe(3)–Fe(2)	86.36 (9)	Fe(6)–Fe(5)–Fe(4)	84.9 (1)
Fe(8)–Fe(7)–Fe(6)	83.9 (1)	Fe(8)–Fe(9)–Fe(1′)	90.33 (9)
		S–Fe–S	
		(μ_2-S)–Fe–(μ_2-S)	
S(2)–Fe(1)–S(1)	104.0 (2)	S(13′)–Fe(1)–S(1)	114.8 (2)
S(13′)–Fe(1)–S(1)	114.8 (2)	S(2)–Fe(2)–S(1)	104.5 (2)
S(3)–Fe(2)–S(1)	115.1 (2)	S(3)–Fe(2)–S(2)	113.8 (2)
S(5)–Fe(3)–S(3)	120.0 (2)	S(7)–Fe(5)–S(5)	119.3 (2)
S(9)–Fe(6)–S(7)	118.8 (2)	S(11)–Fe(7)–S(9)	120.6 (2)
S(13)–Fe(9)–S(11)	118.6 (2)		
		(μ_3-S)–Fe–(μ_2-S)	
S(14′)–Fe(1)–S(1)	112.4 (2)	S(14′)–Fe(1)–S(2)	107.7 (2)
S(14′)–Fe(1)–S(13′)	103.5 (2)	S(4)–Fe(2)–S(1)	112.2 (2)
S(4)–Fe(2)–S(2)	109.0 (2)	S(4)–Fe(2)–S(3)	102.3 (2)
S(4)–Fe(3)–S(3)	103.2 (2)	S(5)–Fe(3)–S(4)	112.8 (2)
S(6)–Fe(3)–S(3)	113.3 (2)	S(6)–Fe(3)–S(5)	102.3 (2)
S(15)–Fe(4)–S(4)	114.7 (2)	S(15)–Fe(4)–S(6)	115.1 (2)
S(15)–Fe(4)–S(8)	115.3 (2)	S(6)–Fe(5)–S(5)	101.6 (2)
S(7)–Fe(5)–S(6)	116.7 (2)	S(8)–Fe(5)–S(5)	114.2 (2)
S(8)–Fe(5)–S(7)	101.0 (2)	S(8)–Fe(6)–S(7)	103.1 (2)
S(9)–Fe(6)–S(8)	112.9 (2)	S(10)–Fe(6)–S(7)	111.8 (2)
S(10)–Fe(6)–S(9)	101.5 (2)	S(10)–Fe(7)–S(9)	102.9 (2)
S(11)–Fe(7)–S(10)	113.8 (2)	S(12)–Fe(7)–S(9)	114.0 (2)
S(12)–Fe(7)–S(11)	100.9 (2)	S(15)–Fe(8)–S(10)	121.4 (2)
S(15)–Fe(8)–S(12)	111.4 (2)	S(15)–Fe(8)–S(14)	112.4 (2)
S(12)–Fe(9)–S(11)	100.2 (2)	S(13)–Fe(9)–S(12)	114.2 (2)
S(14)–Fe(9)–S(11)	114.2 (2)	S(14)–Fe(9)–S(13)	104.0 (2)
		(μ_3-S)–Fe–(μ_3-S)	
S(6)–Fe(3)–S(4)	104.4 (2)	S(6)–Fe(4)–S(4)	104.0 (2)
S(8)–Fe(4)–S(4)	101.5 (2)	S(8)–Fe(4)–S(6)	104.7 (2)
S(8)–Fe(5)–S(6)	103.6 (2)	S(10)–Fe(6)–S(8)	108.7 (2)
S(12)–Fe(7)–S(10)	103.9 (2)	S(12)–Fe(8)–S(10)	104.3 (2)
S(14)–Fe(8)–S(10)	100.3 (2)	S(14)–Fe(8)–S(12)	105.5 (2)
S(14)–Fe(9)–S(12)	105.2 (2)		
		Fe–S–Fe	
		Fe–(μ_2-S)–Fe	
Fe(2)–S(1)–Fe(1)	75.9 (2)	Fe(2)–S(2)–Fe(1)	75.5 (2)
Fe(3)–S(3)–Fe(2)	76.6 (2)	Fe(5)–S(5)–Fe(3)	74.7 (2)
Fe(6)–S(7)–Fe(5)	75.3 (2)	Fe(7)–S(9)–Fe(6)	74.9 (2)
Fe(9)–S(11)–Fe(7)	74.9 (2)	Fe(9)–S(13)–Fe(1′)	77.1 (2)
Fe(8)–S(15)–Fe(4)	95.3 (2)		
		Fe–(μ_3-S)–Fe	
Fe(3)–S(4)–Fe(2)	72.3 (2)	Fe(4)–S(4)–Fe(3)	73.1 (1)
Fe(4)–S(6)–Fe(3)	74.3 (2)	Fe(5)–S(6)–Fe(3)	71.1 (1)
Fe(5)–S(6)–Fe(4)	73.9 (2)	Fe(5)–S(8)–Fe(4)	73.5 (2)
Fe(6)–S(8)–Fe(5)	72.0 (2)	Fe(7)–S(10)–Fe(6)	71.8 (2)
Fe(8)–S(10)–Fe(7)	74.2 (2)	Fe(8)–S(12)–Fe(7)	74.1 (2)
Fe(9)–S(12)–Fe(7)	72.2 (1)	Fe(9)–S(12)–Fe(8)	73.9 (1)
Fe(9)–S(14)–Fe(1′)	73.1 (2)	Fe(9)–S(14)–Fe(8)	71.7 (1)
Fe(4)–S(4)–Fe(2)	108.3 (2)	Fe(8)–S(10)–Fe(6)	104.2 (2)
Fe(6)–S(8)–Fe(4)	107.3 (2)	Fe(8)–S(14)–Fe(1′)	114.0 (2)

similar to that for the preparation of $(Pr_4N)_6Na_2[\alpha\text{-}Na_2Fe_{18}S_{30}]$,[11] but with replacement of Pr_4N^+ with Bu_4N^+ and MeOH/EtOH solvent with pure EtOH to cope with the higher solubility of the product, the black crystalline compound $(Bu_4N)_6Na_4Fe_{18}S_{30}$ was isolated in 70–75% yield. Cluster assembly presumably follows the same pathway as that for $[\alpha\text{-}Na_2Fe_{18}S_{30}]^{8-}$. This is indicated by identical absorption spectra for the reaction mixtures, in which $[FeS_2]_n^{n-}$ is the spectroscopically detected intermediate.[11] The final product is identified by its absorption spectrum in Figure 4, which is indistinguishable from that of $[\alpha\text{-}Na_2Fe_{18}S_{30}]^{8-}$.

Table IV. Displacements (Å) from the Mean Plane Fe_9(1–9) for $[\beta\text{-}Na_2Fe_{18}S_{30}]^{8-}$

Fe(1)	−0.188	S(1)	−1.449
Fe(2)	−0.265	S(2)	0.929
Fe(3)	0.203	S(3)	0.959
Fe(4)	−0.363	S(4)	−1.586
Fe(5)	0.282	S(5)	−0.309
Fe(6)	0.028	S(6)	1.641
Fe(7)	−0.184	S(7)	1.077
Fe(8)	0.221	S(8)	−1.444
Fe(9)	−0.246	S(9)	−0.917
		S(10)	1.468
Na(1)	−1.349	S(11)	0.393
Na(2)	−2.609	S(12)	−1.685
		S(13)	−1.095
		S(14)	1.438
		S(15)	−0.221

Table V. Comparative Structural Features of the α- and β-Isomers of $[Na_2Fe_{18}S_{30}]^{8-}$

	α^a	β^b
imposed sym	C_i	C_i
$l \times w \times h$, Å	13.32 × 15.98 × 3.30	12.39 × 16.29 × 3.33[c]
Fe_2S_2 rhombs	24	22
shared Fe vertices	6	6
shared edges	24	20
μ_2-S	20	18
μ_3-S	8	12
μ_4-S	2	0
dev from Fe(1–9) plane, Å		
Fe	−0.15 to +0.14	−0.36 to +0.28
S	−1.55 to +1.65	−1.69 to +1.64
Na(1)	−0.15	−1.35
Na(2)	−2.66	−2.61

[a] Reference 11. [b] This work. [c] Height (thickness) = S(6) + S(12) displacements (Table IV).

(b) Structure. As evidenced from microscopic examination, the compound $(Bu_4N)_6Na_4Fe_{18}S_{30}\cdot 8EtOH$ is not isomorphous with previously isolated triclinic $(Pr_4N)_6Na_4Fe_{18}S_{30}\cdot 14MeCN$.[11] It crystallizes in monoclinic space group $P2_1/n$ with one-half anion $[\beta\text{-}Na_2Fe_{18}S_{30}]^{8-}$, three Bu_4N^+, two Na^+, and four EtOH solvate molecules in the asymmetric unit. The structure of the anion as viewed from top and side-on perspectives is presented in Figure 5 and a stereoview is shown in Figure 6. Metric data are collected in Tables II–IV. It is immediately apparent that the anion is also a cyclic cluster that exhibits a pronounced similarity to, but is not identical with, $[\alpha\text{-}Na_2Fe_{18}S_{30}]^{8-}$.

The cluster $[\beta\text{-}Na_2Fe_{18}S_{30}]^{8-}$ is a structural isomer of $[\alpha\text{-}Na_2Fe_{18}S_{30}]^{8-}$ and, as such, shares common features of the overall molecular configuration. It has a centrosymmetric cyclic topology of toroidal shape. In this disc-like cluster, all iron atoms are in distorted tetrahedral FeS_4 units organized into 22 non-planar rhombs with which the cluster is built up by a combination of vertex- and edge-sharing. There are no terminal ligands. Two monosolvated sodium ions Na(1,1′) are contained within the sulfide-rich interior of the cluster, each with four Na–S interactions in the range 2.85–3.05 Å. As its α-isomer, the cluster may be thought of as an inorganic crown thiaether. The Fe(1–9) plane is perfect to within 0.36 Å (Table IV). Two trisolvated sodium ions Na(2,2′) are more loosely associated with the cluster through three Na–S interactions at 2.89–3.19 Å at positions 2.61 Å above and below the Fe(1–9) plane. These atoms are not considered an integral part of the cluster. In the crystal, the clusters are packed in parallel layers intersecting at an angle of 65.9°, with the interlayer species filled by Bu_4N^+ cations and ethanol solvate molecules. Distortions owing to the presence of sodium ions appear to be chiefly responsible for symmetry reduction of the cluster from idealized C_{2h} to crystallographically imposed C_i symmetry.

Structural features of the α- and β-isomers of $[Na_2Fe_{18}S_{30}]^{8-}$ are compared in Table V. In contrast to the α-isomer, which is conceptually constructed by sequential connection of two linear Fe_3S_4 and two Fe_6S_9 units, the β-isomer can be considered to arise

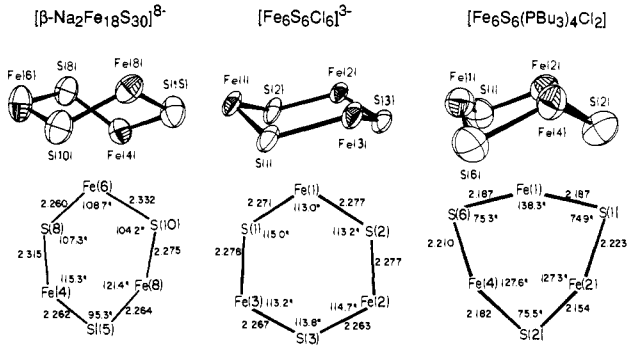

Figure 7. Comparison of Fe_3S_3 ring conformations and dimensions of the skew-boat ring in $[\beta\text{-}Na_2Fe_{18}S_{30}]^{8-}$ and the chair-like rings in the prismane cluster $[Fe_6S_6Cl_6]^{3-}$ [16a] and the basket cluster $Fe_6S_6(PBu_3)_4Cl_2$.[17] The lower rings are projections on Fe_3S_3 mean planes.

Table VI. Mössbauer Spectroscopic Properties of $[\beta\text{-}Na_2Fe_{18}S_{30}]^{8-}$, $[\alpha\text{-}Na_2Fe_{18}S_{30}]^{8-}$, and $[Na_9Fe_{20}Se_{38}]^{9-}$

cluster	T, K	δ,[a] mm/s	ΔE_Q, mm/s	Γ,[b] mm/s	% abs[c]
$[\beta\text{-}Na_2Fe_{18}S_{30}]^{8-}$	4.2	0.33	0.82	0.42	81
		0.53	1.61	0.42	19
	80	0.31	0.81	0.48	84
		0.50	1.52	0.48	16
$[\alpha\text{-}Na_2Fe_{18}S_{30}]^{8-}$ [d]	4.2	0.30	0.81	0.37	83
		0.46	1.49	0.37	17
$[Na_9Fe_{20}Se_{38}]^{9-}$	4.2	0.38	0.58	0.34	66
		0.43	1.12	0.34	34
	80	0.37	0.58	0.36	68
		0.42	1.10	0.36	32
MeCN soln	4.2	0.37	0.55	0.34	64
		0.44	1.03	0.34	36
	80	0.37	0.54	0.36	68
		0.44	1.03	0.36	32

[a] Relative to Fe metal at room temperature. [b] Line width. [c] Percent of total absorption. [d] Reference 11.

from a combination of two Fe_2S_2, four cuboidal Fe_3S_4, and two tetrahedral FeS_4 units. In both isomers, component units have been structurally defined in discrete clusters. Thus, the Fe_2-(1,2)-S_2(1,2) unit closely resembles the cluster core of $[Fe_2S_2L_4]^{2-}$.[26] Edge fusion of three rhombs generates the cuboidal unit $Fe_3(3\text{–}5)S_4(4\text{–}6,8)$, which is known as a protein-bound cluster[14] but has yet to be synthesized as the core of a discrete molecule. The two units are bridged through μ_2-S(3) and μ_3-S(4). This Fe_3S_4 unit is bridged to another, $Fe_3(7\text{–}9)S_4(7,9\text{–}11)$, through tetrahedral Fe(6)S_4(7–10) and μ_2-S(15). The doubly-bridging atoms S(3,7,15) are not part of the constituent Fe_2S_2 and Fe_3S_4 units. Repetition of this pattern produces a ring structure. Adjacent Fe_3S_4 units are disposed such that the unoccupied positions of the site-voided cubane are on opposite sides of the Fe(1–9) plane. In the α-isomer (Figure 1), the four Fe_3S_4 units are contained within two Fe_6S_9 fragments, one of which is $Fe_6(3\text{–}8)S_9(3,5\text{–}12)$. Here the voided sites of adjacent units are on the same side of the Fe(1–9) plane. Consequently, the idealized C_2 axis of the β-isomer passes along the long (major) axis of the disc whereas in the α-isomer it is along the short (minor) axis. Despite the very similar atom spatial arrangements, the two molecules are not superimposable because the ratio major axis/minor axis is 1.20 for the α-isomer and 1.31 for the β-isomer.

Unlike the α-isomer (Figure 1), which is built up entirely from vertex- and edge-shared Fe_2S_2 rhombs, the β-isomer contains the atoms S(15,15′) which do not belong to any rhombs. Consequently, the structure accommodates two Fe_3S_3 rings and is the second example of a Fe–S cluster not built up entirely by the sharing of Fe_2S_2 rhombs. The basket clusters $Fe_6S_6(PR_3)_4L_2$ (L = RS^-, halide)[13,17] and $[Fe_6S_6(PEt_3)_6]^{+}$ [27] contain such rings. The

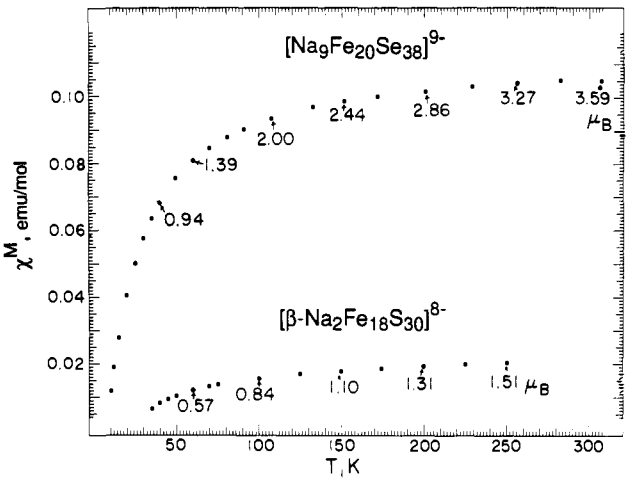

Figure 8. Temperature dependence of the molar magnetic susceptibilities (corrected for diamagnetism) of $[\beta\text{-}Na_2Fe_{18}S_{30}]^{8-}$ (lower) and $[Na_9Fe_{20}Se_{38}]^{9-}$ (upper); values of μ_{Fe} (μ_B) at selected temperatures are indicated.

prismane clusters $[Fe_6S_6L_6]^{3-}$ (L = RO^-, RS^-, halide)[16] also possess Fe_3S_3 rings, but all atoms therein are included in rhombs. The structures of these six-membered rings are compared in Figure 7, from which it is seen that the ring in $[\beta\text{-}Na_2Fe_{18}S_{30}]^{8-}$ has the skew-boat conformation. This conformation and ring dimensions are far closer to those of the prismane cluster than to those of the irregular ring of the basket cluster. It appears unlikely that the ring conformation will permit a reaction analogous to the capping of prismane faces by the formation of three M–S bonds, as has been accomplished.[28] A more likely prospect is the bridging of S(15,15′), separated by 4.08 Å, by metal ions.

(c) Electronic Features. The Mössbauer spectra of $[\beta\text{-}Na_2Fe_{18}S_{30}]^{8-}$ was examined in zero-field at 4.2–80 K and under a longitudinally applied field of 80 kOe at 4.2 K. Isomer shifts (δ) and quadrupole splittings (ΔE_Q) are contained in Table VI. The spectra (not shown) are virtually the same as those for $[\alpha\text{-}Na_2Fe_{18}S_{30}]^{8-}$,[11] as would be expected from the isomeric structures and the same mean iron oxidation state. They show two apparent overlapping quadrupole doublets, with the minority doublet appearing as a shoulder on the high velocity side. No magnetic hyperfine structure was observed in zero-field, and the magnetically perturbed spectrum consisted of a typical four-line pattern for a diamagnetic species in a longitudinal field.

$[\beta\text{-}Na_2Fe_{18}S_{30}]^{8-}$ is a mixed-valence cluster formally containing 14Fe(III) + 4Fe(II) and having nine crystallographically distinct iron sites. Subspectra for these sites are not resolved, and individual Fe(II) sites, for which $\delta \approx 0.7$ mm/s and $\Delta E_Q \approx 3$ mm/s are expected,[29] are not observed. Spectral parameters based on a two-site fit are given in Table VI together with those for the α-isomer at 4.2 K. With use of the empirical relationship between isomer shifts and oxidation states for tetrahedral FeS_4 sites,[30] the majority doublet corresponds to the oxidation state 2.85+ and the minority doublet to 2.39+. The weighted average of 2.76+ agrees well with the value of 2.78+ from the chemical formula. While the cluster is electronically delocalized, the electronic distribution is not uniform. We observe that the sites Fe(4.8)(μ_2-S)(μ_3-S)$_3$ (Figure 4) have the highest bridging multiplicity and the longest mean bond lengths (2.29–2.30 Å). They offer the least electron-rich coordination environment and would be most hospitable to the Fe(II) state. The sites Fe(1,2)(μ_2-S)$_3$(μ_3-S), on the other hand, have the lowest bridging multiplicity and the shortest mean bond distances (2.24 Å), and should be most effective in localizing

(26) Berg, J. M.; Holm, R. H. In *Iron-Sulfur Proteins*; Spiro, T. G., Ed.; Wiley-Interscience: New York, 1982; Chapter 1.
(27) Snyder, B. S.; Holm, R. H. *Inorg. Chem.* **1990**, *29*, 274.
(28) Al-Ahmad, S. A.; Salifoglou, A.; Kanatzidis, M. G.; Dunham, W. R.; Coucouvanis, D. *Inorg. Chem.* **1990**, *29*, 927 and references therein.
(29) Lane, R. W.; Ibers, J. A.; Frankel, R. B.; Papaefthymiou, G. C.; Holm, R. H. *J. Am. Chem. Soc.* **1977**, *99*, 84.
(30) Christou, G.; Mascharak, P. K.; Armstrong, W. H.; Papaefthymiou, G. C.; Frankel, R. B.; Holm, R. H. *J. Am. Chem. Soc.* **1982**, *104*, 2820.

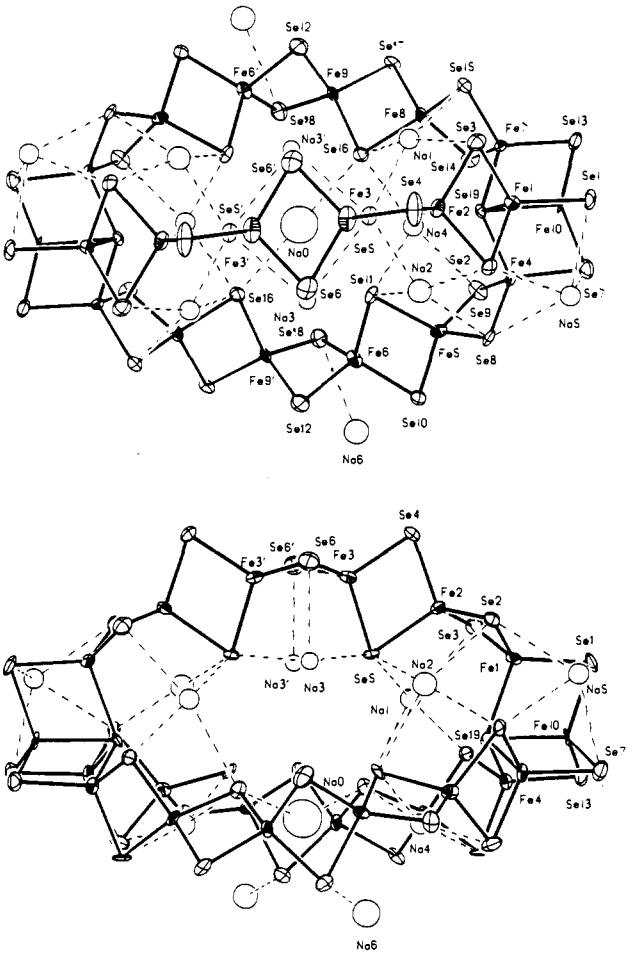

Figure 9. Two views of the structure of $[Na_9Fe_{20}Se_{38}]^{9-}$ showing 70% probability ellipsoids (Fe and Se atoms) and the atom-labeling scheme. Primed and unprimed atoms are related by an imposed C_2 axis passing through Na(0) and perpendicular to the mean plane of the $Fe_2(3,3')$-$Se_2(6,6')$ rhomb. The two views differ by a 90° rotation around the idealized C_3 axis which contains Fe(10,10').

oxidation states near Fe(III). The remaining sites are intermediate between these two extremes. The patterns of electron delocalization of the two isomers are very similar. The 14 iron sites in the molecular periphery tend toward Fe(III) while the four sites in the interior approach Fe(II).

The temperature dependence of the magnetic susceptibility of $[\beta\text{-}Na_2Fe_{18}S_{30}]^{8-}$, plotted in Figure 8, is indicative of antiferromagnetism and a singlet ground state and is consistent with the Mössbauer results. The magnetic moment per iron atom at 250 K, $\mu_{Fe} = 1.51\ \mu_B$, is somewhat larger than that of the α-isomer at 267 K (1.28 μ_B) and is comparable with room-temperature moments for $[Fe_2S_2(SR)_4]^{2-}$ (1.4 μ_B[31]), $[Fe_4S_4(SR)_4]^{2-}$ (1.1 μ_B[32]), and $[Fe_6S_9(SR)_2]^{4-}$ (1.1–1.2 μ_B[33]). Both cyclic clusters, as all other iron–sulfur clusters, are overall antiferromagnetically coupled.

(d) Redox. Cyclic voltammograms of $[\beta\text{-}Na_2Fe_{18}S_{30}]^{8-}$ (not shown) reveal redox properties very similar to, but distinguishable from, those of the α-isomer.[11] Two oxidations are observed at $E_{1/2} = -0.67$ V (quasireversible) and −0.43 V (chemically reversible), compared to −0.62 and −0.37 V for the α-isomer. These steps are followed at more positive potentials by multielectron oxidations, a common behavior of Fe–S/Se clusters. One or two irreversible reductions are observed at $E_{pc} = -1.5$ to −1.6 V and a coupled anodic step occurs at $E_{pa} = -1.27$ V. For [α-

(31) Gillum, W. O.; Frankel, R. B.; Foner, S.; Holm, R. H. *Inorg. Chem.* **1976**, *15*, 1095.
(32) Papaefthymiou, G. C.; Laskowski, E. J.; Frota-Pessoa, S.; Frankel, R. B.; Holm, R. H. *Inorg. Chem.* **1982**, *21*, 1723.
(33) Strasdeit, H.; Krebs, B.; Henkel, G. *Inorg. Chem.* **1984**, *23*, 1816.

Table VII. Selected Interatomic Distances (Å) for $[Na_9Fe_{20}Se_{38}]^{9-}$[a]

		Fe···Fe	
		In $Fe_6(\mu_2\text{-Se})_{10}$ Chain	
Fe(1)–Fe(2)	2.755 (7)	Fe(2)–Fe(3)	2.855 (7)
Fe(4)–Fe(5)	2.784 (7)	Fe(5)–Fe(6)	2.789 (7)
Fe(7)–Fe(8)	2.744 (7)	Fe(8)–Fe(9)	2.843 (7)
mean	2.76 (2)	mean	2.83 (3)
Fe(3)–Fe(3′)	2.78 (1)		
Fe(6)–Fe(9′)	2.760 (7)		
mean	2.766 (9)		
		In $Fe_4(\mu_2\text{-Se})_3(\mu_4\text{-Se})$ Bridgehead	
Fe(1)–Fe(10)	2.864 (7)		
Fe(4)–Fe(10)	2.887 (8)		
Fe(7)–Fe(10)	2.869 (7)		
mean	2.873 (10)		
		Fe–(μ_2-Se)	
		In $Fe_6(\mu_2\text{-Se})_{10}$ Chain	
Fe(1)–Se(2)	2.361 (7)	Fe(2)–Se(2)	2.369 (7)
Fe(1)–Se(3)	2.335 (7)	Fe(2)–Se(3)	2.372 (7)
Fe(4)–Se(8)	2.380 (7)	Fe(5)–Se(8)	2.380 (6)
Fe(4)–Se(9)	2.324 (7)	Fe(5)–Se(9)	2.376 (7)
Fe(7)–Se(14)	2.349 (6)	Fe(8)–Se(14)	2.362 (7)
Fe(7)–Se(15)	2.339 (7)	Fe(8)–Se(15)	2.369 (6)
mean	2.35 (2)	mean	2.371 (6)
Fe(2)–Se(4)	2.340 (6)	Fe(2)–Se(5)	2.436 (6)
Fe(5)–Se(10)	2.335 (7)	Fe(5)–Se(11)	2.428 (7)
Fe(8)–Se(17)	2.359 (7)	Fe(8)–Se(16)	2.399 (7)
mean	2.345 (10)	mean	2.42 (2)
Fe(3)–Se(4)	2.347 (6)	Fe(3)–Se(5)	2.422 (6)
Fe(6)–Se(10)	2.329 (7)	Fe(6)–Se(11)	2.374 (7)
Fe(9)–Se(17)	2.364 (6)	Fe(9)–Se(16)	2.383 (7)
mean	2.345 (14)	mean	2.39 (2)
Fe(3)–Se(6)	2.371 (8)		
Fe(3)–Se(6′)	2.371 (8)		
Fe(6)–Se(12)	2.384 (7)		
Fe(6)–Se(18′)	2.407 (6)		
Fe(9)–Se(12′)	2.365 (7)		
Fe(9)–Se(18)	2.351 (6)		
mean	2.38 (2)		
		Fe–(μ_2-Se)	
		In $Fe_4(\mu_2\text{-Se})_3(\mu_4\text{-Se})$ Bridgehead	
Fe(1)–Se(1)	2.333 (6)	Fe(10)–Se(1)	2.376 (7)
Fe(4)–Se(7)	2.315 (6)	Fe(10)–Se(7)	2.380 (7)
Fe(7)–Se(13)	2.296 (7)	Fe(10)–Se(13)	2.356 (7)
mean	2.32 (2)	mean	2.371 (10)
		Fe–(μ_4-Se)	
		In $Fe_4(\mu_2\text{-Se})_3(\mu_4\text{-Se})$ Bridgehead	
Fe(1)–Se(19)	2.542 (6)	Fe(10)–Se(19)	2.439 (6)
Fe(4)–Se(19)	2.517 (7)		
Fe(7)–Se(19)	2.522 (6)		
mean	2.527 (11)		
		Se···Na (EtOH)	
Se(16)–Na(0)	3.00 (1)	Se(5)–Na(3)	3.14 (1)
Se(3)–Na(1)	2.93 (2)	Se(5′)–Na(3)	3.09 (1)
Se(5)–Na(1)	2.96 (2)	Se(6)–Na(3)	2.99 (1)
Se(15)–Na(1)	2.95 (2)	Se(9)–Na(4)	2.91 (2)
Se(16)–Na(1)	3.05 (2)	Se(11)–Na(4)	2.96 (2)
Se(2)–Na(2)	2.87 (2)	Se(14)–Na(4)	2.95 (2)
Se(5)–Na(2)	2.89 (2)	Se(16)–Na(4)	2.95 (2)
Se(8)–Na(2)	2.89 (2)	Se(6)–Na(7)	2.86 (8)
Se(11)–Na(2)	2.94 (2)	Se(10)–Na(6)	3.40 (1)
Se(19)–Na(4)	3.27 (2)	Se(18)–Na(6)	3.31 (1)
		Se···Na (MeC(O)NHPh)	
Se(1)–Na(5)	3.00 (2)	Se(2)–Na(5)	3.14 (2)
Se(7)–Na(5)	3.05 (2)	Se(8)–Na(5)	3.12 (1)
		Na···Na	
Na(0)–Na(4)	3.51 (1)	Na(0)–Na(4)	3.51 (1)
Na(1)–Na(3)	3.71 (2)	Na(2)–Na(3)	3.45 (2)
Na(6)–Na(6′)	3.52 (3)	Na(3)–Na(3′)	4.60 (2)
		Na···O (EtOH)	
Na(0)–O(4)	2.39 (4)	Na(1)–O(1)	2.40 (3)
Na(2)–O(2)	2.42 (3)	Na(3)–O(1)	2.39 (3)
Na(3)–O(2)	2.35 (3)	Na(4)–O(4)	2.40 (3)
Na(6)–O(6)	2.48 (3)	Na(6)–O(6′)	2.32 (3)
Na(6)–O(7)	2.43 (3)	Na(6)–O(8)	2.30 (3)
Na(7)–O(9)	2.58 (6)	Na(7)–O(9′)	2.58 (6)
Na(7)–O(10)	2.33 (7)	Na(7)–O(10′)	2.33 (7)
		Na···O (MeC(O)NHPh)	
Na(5)–O(5)	2.18 (3)		

[a] The data are organized under idealized D_{3h} symmetry.

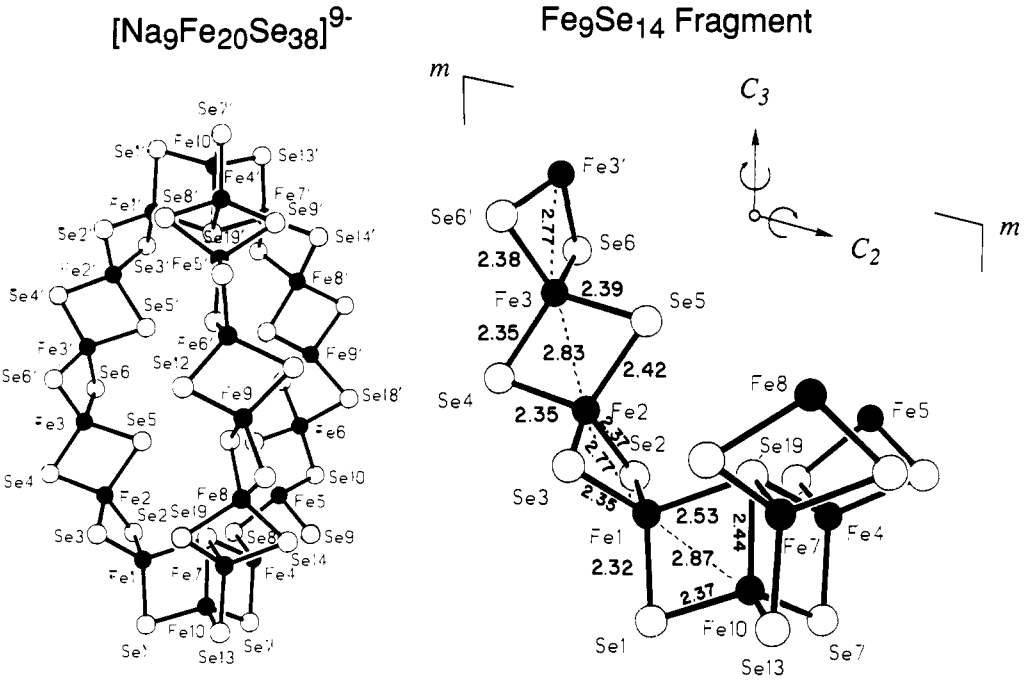

Figure 10. Left: structure of $[Na_9Fe_{20}Se_{38}]^{9-}$. Right: an enlarged view of an Fe_9Se_{14} fragment, independent under idealized D_{3h} symmetry, showing the three bridgehead rhombs fused along a common edge and the attachment of one of the three Fe_6Se_{10} chains to the bridgehead. Sodium ions are omitted for clarity. The locations of several D_{3h} symmetry elements are indicated; interatomic distances are averaged under this symmetry.

$Na_2Fe_{18}S_{30}]^{8-}$, reductions occur in the same range but the oxidation feature occurs at −0.97 V. The reduction sites are perhaps the cuboidal Fe_3S_4 fragments which, as just noted, may be suitable for the stabilization of Fe(II).

$[Na_9Fe_{20}Se_{38}]^{9-}$. (a) Cluster Synthesis. Replacement of Li_2S with Li_2Se in the assembly system of Figure 3 results in a brown solution with a broad, featureless absorption spectrum of unknown origin when $n \leq 1.2$ and a dark brownish-green mixture when $1.2 < n < 2.1$. The absorption spectrum of the latter, with its four bands at 353, 446, 558, and 673 nm (Figure 3), is a red-shifted version of the spectrum of $[FeS_2]_n^{n-}$ (335, 425, 530, 618 nm); its intensity increases when the number of equivalents of Li_2Se is increased above $n = 1.2$. Accordingly, this spectrum is assigned to the polymer $[FeSe_2]_n^{n-}$. Addition of the precipitant Bu_4N^+ caused slow conversion of the intermediate to the final product, which was isolated as a black crystalline product in 70% yield. The absorption spectrum of this material (Figure 4) is dissimilar to that of either isomer of $[Na_2Fe_{18}S_{30}]^{8-}$, suggesting a different structure.

(b) Structure. Compound B in Table I crystallizes in orthorhombic space group *Pbcn* with one-half anion $[Na_9Fe_{20}Se_{38}]^{9-}$, two and one-quarter Bu_4N^+, two and one-quarter Na^+, one acetanilide, and seven and one-half ethanol molecules in the asymmetric unit. The nonstoichiometric formula arises from a half interstitial ethanol molecule and a model based on a 1:1 occupancy. That ethanol and acetanilide are present as protonated molecules was inferred from bond distances and angles to nearby Na^+ cations. These molecules and the quaternary ammonium cations (with the exception of a few disordered carbon atoms) were generally well-ordered and unexceptional and are not considered further. The composition of compound B is further supported by analysis for all elements except oxygen and the Se:Fe atom ratio by EDS. Several views of the cluster structure are presented in Figures 9 and 10 and a stereoview is given in Figure 6. Metric data are collected in Tables VII–IX.

As the α and β forms of $[Na_2Fe_{18}S_{30}]^{8-}$, the cluster $[Na_9Fe_{20}Se_{38}]^{9-}$ possesses two remarkable structural features. It contains *no terminal ligands*, thus necessitating a cyclic Fe–Se framework. But unlike the monocyclic isomers, $[Na_9Fe_{20}Se_{38}]^{9-}$ is a *bicyclic* cluster of ellipsoidal shape. It is the only bicyclic cluster. Within the cluster cavity are encapsulated nine sodium ions Na(0–4,1′–4′), which are additionally coordinated to a total of eight ethanol molecules. The cluster has a prolated ellipsoidal topology with dimensions 11.2 × 17.4 Å, placing it in the nanometer size range. The minor axis is twice the centroid–Se(6) distance and the major axis is the Se(1)–Se(1′) distance. The cluster has imposed C_2 symmetry, with the 2-fold axis passing through Na(0) and perpendicular to the mean plane of rhomb $Fe_2(3,3')Se_2(6,6')$, and, as will be seen, approaches idealized D_{3h} symmetry.

The structure is built up entirely from 21 Fe_2Se_2 rhombs, 15 of which share iron vertices to form three separate but essentially equivalent $Fe_6(\mu_2\text{-Se})_{10}$ chains. The cluster has 36 μ_2-Se atoms, 2 μ_4-Se atoms, 15 vertex-sharing Fe_2Se_2 rhombs, and 6 edge-sharing rhombs, with all iron atoms in distorted tetrahedral $FeSe_4$ sites. The chains contain the atoms Fe(1–3,3′–1′), Fe(7–9,6′–4′), and Fe(4–6,9′–7′) and are positioned roughly parallel to an idealized C_3 axis that contains Fe(10,10′). These chains are particularly apparent when sodium ions are removed from the structure (Figure 10). The terminal atoms Fe(1,4,7) at one end are included in bridgehead rhombs by three additional μ_2-Se(1,7,13) bridges which also connect to Fe(10). Atoms Fe(1,4,7,10) are bridged by μ_4-Se(19). In this way, three bridgehead rhombs $Fe_2(7,10)Se_2(13,19)$, $Fe_2(1,10)Se_2(1,19)$, and $Fe_2(4,10)Se_2(7,19)$ are formed and share the common edge Fe(10)–Se(19). A symmetry-related bridgehead unit completes the structure on the opposite end.

The nature of the Fe_6S_{10} chains is described in terms of the independent atoms of one of them. With reference to Table IX and Figure 10, the plane containing atoms Fe(1–3) and bridgehead atom Fe(10) is perfect to ±0.122 Å. The atoms Se(1,19) in the bridgehead and Se(4,5) in the chain show comparably small deviations from this plane. Above and below the Fe(1–3,10) plane, sandwiching it at a distance of 2.1 Å, are two uneven planes of atoms 1.1 Å thick. These contain the bridgehead atoms Fe(4,7), four interior sodium atoms, and nine selenium atoms, three of which, Se(2,3,6), are from Fe_2Se_2 rhombs in the chain that are perpendicular to the Fe(1–3,10) plane. The other six selenium atoms are from the other two chains. The displacements of atoms in the sandwich layers and of other atoms in Table IX convey the size of the cluster cavity defined by the chains and the separation of chains. The two related planes from other chains, Fe(4–6,10) and Fe(7–9,10), intersect the first with dihedral angles of 120.0°.

A cluster fragment Fe_9Se_{14}, independent under idealized D_{3h} symmetry, is shown in enlarged form in Figure 10 in order to make clear the way in which the chains are anchored in the bridgehead region. The close approach to idealized D_{3h} symmetry is emphasized by the minor variation of two of the three dihedral angles

Table VIII. Selected Bond Angles (deg) for $[Na_9Fe_{20}Se_{38}]^{9-}$ [a]

Fe–Fe–Fe			
In $Fe_6(\mu_2\text{-Se})_{10}$ Chain			
Fe(3)–Fe(2)–Fe(1)	164.6 (2)	Fe(3′)–Fe(3)–Fe(2)	161.0 (1)
Fe(6)–Fe(5)–Fe(4)	162.1 (3)	Fe(9′)–Fe(6)–Fe(5)	159.2 (3)
Fe(9)–Fe(8)–Fe(7)	163.8 (3)	Fe(8)–Fe(9)–Fe(6′)	160.1 (3)
In $Fe_4(\mu_2\text{-Se})_3(\mu_4\text{-Se})$ Bridgehead			
Fe(10)–Fe(1)–Fe(2)	157.3 (2)	Fe(4)–Fe(10)–Fe(1)	92.2 (2)
Fe(10)–Fe(7)–Fe(8)	156.7 (3)	Fe(7)–Fe(10)–Fe(1)	92.2 (2)
Fe(10)–Fe(4)–Fe(5)	157.7 (3)	Fe(7)–Fe(10)–Fe(4)	91.4 (2)
$(\mu_2$-Se)–Fe–$(\mu_2$-Se)			
In $Fe_6(\mu_2\text{-Se})_{10}$ Chain			
Se(2)–Fe(1)–Se(1)	111.4 (3)	Se(4)–Fe(2)–Se(2)	110.7 (3)
Se(3)–Fe(1)–Se(1)	117.6 (3)	Se(4)–Fe(2)–Se(3)	113.1 (3)
Se(8)–Fe(4)–Se(7)	112.3 (3)	Se(10)–Fe(5)–Se(8)	112.2 (3)
Se(9)–Fe(4)–Se(7)	115.9 (3)	Se(10)–Fe(5)–Se(9)	111.9 (2)
Se(14)–Fe(7)–Se(13)	114.7 (3)	Se(17)–Fe(8)–Se(14)	110.4 (2)
Se(15)–Fe(7)–Se(13)	115.0 (3)	Se(17)–Fe(8)–Se(15)	111.9 (3)
Se(3)–Fe(1)–Se(2)	106.2 (2)	Se(3)–Fe(2)–Se(2)	104.8 (2)
Se(9)–Fe(4)–Se(8)	105.2 (3)	Se(9)–Fe(5)–Se(8)	103.6 (2)
Se(15)–Fe(7)–Se(14)	106.3 (2)	Se(15)–Fe(8)–Se(14)	104.9 (2)
Se(5)–Fe(2)–Se(2)	111.4 (3)	Se(6)–Fe(3)–Se(4)	114.0 (3)
Se(5)–Fe(2)–Se(3)	110.6 (3)	Se(6′)–Fe(3)–Se(4)	112.1 (3)
Se(11)–Fe(5)–Se(8)	111.4 (2)	Se(12)–Fe(6)–Se(10)	110.4 (3)
Se(11)–Fe(5)–Se(9)	111.8 (3)	Se(18′)–Fe(6)–Se(10)	114.3 (3)
Se(16)–Fe(8)–Se(15)	110.3 (2)	Se(17)–Fe(9)–Se(12′)	113.1 (3)
Se(16)–Fe(8)–Se(14)	113.7 (3)	Se(18)–Fe(9)–Se(17)	109.2 (2)
Se(5)–Fe(2)–Se(4)	106.4 (2)	Se(5)–Fe(3)–Se(4)	106.6 (2)
Se(11)–Fe(5)–Se(10)	106.1 (2)	Se(11)–Fe(6)–Se(10)	108.1 (2)
Se(17)–Fe(8)–Se(16)	105.7 (2)	Se(17)–Fe(9)–Se(16)	106.1 (2)
Se(6)–Fe(3)–Se(5)	110.1 (3)	Se(6)–Fe(3)–Se(6′)	104.2 (2)
Se(6′)–Fe(3)–Se(5)	109.9 (3)	Se(18′)–Fe(6)–Se(12)	102.9 (2)
Se(12)–Fe(6)–Se(11)	113.3 (3)	Se(18)–Fe(9)–Se(12′)	105.2 (2)
Se(18′)–Fe(6)–Se(11)	107.9 (3)		
Se(16)–Fe(9)–Se(12′)	109.6 (3)		
Se(18)–Fe(9)–Se(16)	113.8 (3)		
In $Fe_4(\mu_2\text{-Se})_3(\mu_4\text{-Se})$ Bridgehead			
Se(7)–Fe(10)–Se(1)	109.2 (3)		
Se(13)–Fe(10)–Se(1)	111.4 (3)		
Se(13)–Fe(10)–Se(7)	113.8 (3)		
mean	112 (2)		
$(\mu_4$-Se)–Fe–$(\mu_2$-Se)			
In $Fe_4(\mu_2\text{-Se})_3(\mu_4\text{-Se})$ Bridgehead			
Se(19)–Fe(1)–Se(1)	106.4 (2)	Se(19)–Fe(1)–Se(2)	105.8 (2)
Se(19)–Fe(4)–Se(7)	106.2 (3)	Se(19)–Fe(1)–Se(3)	108.7 (2)
Se(19)–Fe(10)–Se(13)	107.0 (2)	Se(19)–Fe(4)–Se(8)	105.6 (2)
mean	106.5 (3)	Se(19)–Fe(4)–Se(9)	111.2 (3)
		Se(19)–Fe(7)–Se(14)	105.7 (2)
Se(19)–Fe(10)–Se(1)	108.4 (2)	Se(19)–Fe(7)–Se(15)	108.4 (2)
Se(19)–Fe(10)–Se(7)	106.7 (2)	mean	108 (2)
Se(19)–Fe(7)–Se(13)	106.2 (3)		
mean	107.1 (9)		
Fe–$(\mu_2$-Se)–Fe			
In $Fe_6(\mu_2\text{-Se})_{10}$ Chain			
Fe(2)–Se(2)–Fe(1)	71.3 (2)	Fe(3)–Se(6)–Fe(3′)	71.9 (2)
Fe(2)–Se(3)–Fe(1)	71.6 (2)	Fe(9′)–Se(12)–Fe(6)	71.0 (2)
Fe(5)–Se(8)–Fe(4)	71.6 (2)	Fe(9)–Se(18)–Fe(6′)	70.9 (2)
Fe(5)–Se(9)–Fe(4)	72.6 (2)	mean	71.3 (4)
Fe(8)–Se(14)–Fe(7)	71.3 (2)		
Fe(8)–Se(15)–Fe(7)	71.3 (2)		
mean	71.6 (5)		
Fe(3)–Se(4)–Fe(2)	75.0 (2)	Fe(3)–Se(5)–Fe(2)	72.0 (2)
Fe(6)–Se(10)–Fe(5)	73.4 (2)	Fe(6)–Se(11)–Fe(5)	71.0 (2)
Fe(9)–Se(17)–Fe(8)	74.0 (2)	Fe(9)–Se(16)–Fe(8)	73.0 (2)
mean	74.1 (7)	mean	72.0 (8)
In $Fe_4(\mu_2\text{-Se})_3(\mu_4\text{-Se})$ Bridgehead			
Fe(10)–Se(1)–Fe(1)	74.9 (2)		
Fe(10)–Se(7)–Fe(4)	75.9 (2)		
Fe(10)–Se(13)–Fe(7)	76.1 (2)		
mean	75.6 (5)		
Fe–$(\mu_4$-Se)–Fe			
In $Fe_4(\mu_2\text{-Se})_3(\mu_4\text{-Se})$ Bridgehead			
Fe(10)–Se(19)–Fe(1)	70.2 (2)	Fe(4)–Se(19)–Fe(1)	110.0 (2)
Fe(10)–Se(19)–Fe(4)	71.3 (2)	Fe(7)–Se(19)–Fe(1)	109.3 (2)
Fe(10)–Se(19)–Fe(7)	70.6 (2)	Fe(7)–Se(19)–Fe(4)	109.6 (2)
mean	70.7 (5)	mean	109.6 (3)

[a] The data are organized under idealized D_{3h} symmetry.

Table IX. Dihedral Angles (deg) and Displacements (Å) from the Mean Plane Fe_4(1–3, 10) for $[Na_9Fe_{20}Se_{38}]^{9-}$

Dihedral Angles between Bridgehead Rhombs	
$Fe_2(1,10)Se_2(1,19)/Fe_2(4,10)Se_2(7,19)$	120.0
$Fe_2(1,10)Se_2(1,19)/Fe_2(7,10)Se_2(13,19)$	119.5
$Fe_2(4,10)Se_2(7,19)/Fe_2(7,10)Se_2(13,19)$	120.5

in-plane		sandwich layer		other	
Fe(1)	−0.074	Fe(4)	2.247	Fe(5)	3.685
Fe(2)	−0.108	Fe(7)	−1.859	Fe(6)	4.322
Fe(3)	−0.038			Fe(8)	−3.029
Fe(10)	0.122	Se(2)	1.777	Fe(9)	−3.962
		Se(3)	−1.974		
Se(1)	0.053	Se(6)	1.872	Se(8)	3.985
Se(4)	−0.134	Se(7)	2.184	Se(10)	5.714
Se(5)	−0.058	Se(9)	2.562	Se(12)	5.484
Se(19)	0.099	Se(11)	2.371	Se(15)	−3.812
		Se(13)	−1.779	Se(17)	−4.795
Na(0)	0.000	Se(14)	−1.576	Se(18)	−3.625
Na(4)	0.384	Se(16)	−1.975		
				Na(6)	6.717
		Na(1)	−2.284		
		Na(2)	2.341		
		Na(3)	2.299		
		Na(5)	2.911		

between bridgehead rhombs from 120° (Table IX). This symmetry is broken mainly by small twists in the three Fe_6Se_{10} chains and by the disposition of atoms Na(0,3,3′) in the cluster interior.

Because of the large number of independent parameters, the metric data in Tables VII and VIII are organized under D_{3h} symmetry. Most values are unexceptional when compared to molecular Fe–Se clusters.[25,34,35] However, the alternation of mean Fe–Fe distances in the Fe_6Se_{10} chains (2.87, 2.76, 2.83, 2.77 Å; Table VII) is somewhat unusual and is absent in either isomer of $[Na_2Fe_{18}S_{30}]^{8-}$, and in the linear clusters $[Fe_3Q_4(SPh)_4]^{3-}$ [35,36] and $[Fe_4S_6(SEt)_6]^{4-}$.[37] In $[Fe_3Se_4(SPh)_4]^{3-}$ the Fe–Fe distance is 2.781 (1) Å.[35] The effect is due mainly to the considerably larger nonplanar distortions in Fe_2Se_2 rhombs having shorter Fe–Fe distances than those having longer Fe–Fe distances. Mean values of dihedral angles between $FeSe_2$ portions over the entire structure are 34.2° and 5.9° for rhombs with short and long Fe–Fe distances, respectively.

The large interchain space with a selenide-rich interior provides a negatively charged cavity that encapsulates the nine sodium ions Na(0,1–4,1′–4′). The majority of these ions make four strong bonding interactions with selenide atoms over the range 2.87 (2)–3.14 (1) Å. Exceptions are Na(0), which has two such contacts with Se(16,16′). The ions Na(3,3′), Fe(3,3′), and Se(5,6,5′,6′) give rise to a unique $[Na_2Fe_2Se_4]$ cubane-type substructure. In addition to four strong contacts with neighboring selenides, the ions Na(4,4′) enter into weaker interactions with Se(19,19′) at 3.27 (2) Å. The remaining four sodium ions Na(5,5′,6,6′) are associated with the exterior of the cluster and are involved in other bonding interactions. Na(5,5′) are each coordinated to one acetanilide molecule. Na(6,6′) are each terminally coordinated to two ethanol molecules and bridged by two ethanol molecules to sodium ions exterior to another cluster related by an inversion symmetry, forming an infinite unidimensional network in which the clusters are arrayed in a parallel fashion. The majority of Na–Se interactions are evident in Figure 9. Its bicyclic nature and the inclusion of sodium ions in its interior distinguish the cluster as an inorganic thiacryptand.

(34) (a) Bobrik, M. A.; Laskowski, E. J.; Johnson, R. W.; Gillum, W. O.; Berg, J. M.; Hodgson, K. O.; Holm, R. H. *Inorg. Chem.* **1978**, *17*, 1402. (b) Rutchik, S.; Kim, S.; Walters, M. A. *Inorg. Chem.* **1988**, *27*, 1515. (c) Strasdeit, H.; Krebs, B.; Henkel, G. *Z. Naturforsch.* **1987**, *42b*, 565.

(35) Yu, S.-B.; Papaefthymiou, G. C.; Holm, R. H. *Inorg. Chem.* **1991**, *30*, 3476 and references therein.

(36) Hagen, K. S.; Watson, A. D.; Holm, R. H. *J. Am. Chem. Soc.* **1983**, *105*, 3905.

(37) Al-Ahmad, S. A.; Kampf, J. W.; Dunham, W. R.; Coucouvanis, D. *Inorg. Chem.* **1991**, *30*, 1164.

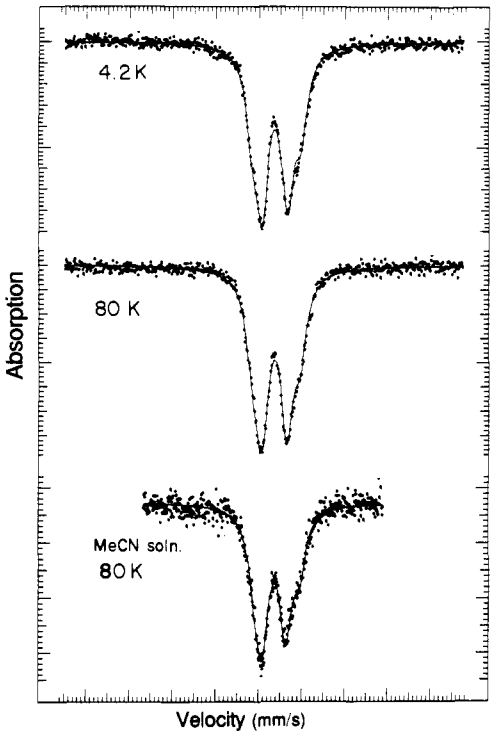

Figure 11. Mössbauer spectra of $[Na_9Fe_{20}Se_{38}]^{9-}$ in the solid state at 4.2 and 80 K, and in acetonitrile solution at 80 K.

The Fe:Se ratio of 0.526 is the lowest of any molecular Fe–S/Se cluster and approaches the value of 0.5 for M^IFeQ_2 phases (Q = S, Se).[38] These contain tetrahedral edge-shared $^1_\infty[FeQ_2]$ chains, which is the prevalent bridging modality for all-Fe(III) chalcogenide solid-state molecular compounds.[39] Other examples include $[Fe_3Q_4(SR)_4]^{3-}$,[35,36] $[Fe_4S_6(SR)_4]^{4-}$,[37] and $[Fe_2Q_6]^{6-}$ in Na_3FeQ_3.[40] This bridging arrangement is also present in compounds such as $Ba_9Fe_{16}S_{32}$[41] and $Na_3Fe_2S_4$,[42] which contain one-half or more Fe(III), although the latter compound is not notably stable. The low Fe:Se ratio for $[Na_9Fe_{20}Se_{38}]^{9-}$ reflects the fact that edge-shared $[FeSe_2]^-$ units in Fe_2Se_2 rhombs constitute the main building block of the cluster, a matter that could otherwise be safely inferred from the conspicuous spectral similarity of the cluster and $[FeSe_2]_n^{n-}$ (Figure 4).

(c) Electronic Features. The Mössbauer spectra of $[Na_9Fe_{20}Se_{38}]^{9-}$ were obtained in zero-field at 1.6–180 K and under a longitudinally applied field of 80 kOe at 4.2 K. Spectra of solid and solution samples are shown in Figure 11. They consist of two apparent overlapping doublet features, with the minority doublet appearing as a shoulder on the high velocity side. No magnetic hyperfine structure was observed, discounting the most likely impurities, $NaFeS_2$ or $(Bu_4N)FeSe_2$, as responsible for the minority doublet. These compounds, as their sulfide analogues, are expected to show six-line magnetic hyperfine structure. The magnetically perturbed solid-state spectrum consists of the usual four-line pattern for diamagnetic species. All Mössbauer observations are consistent with a singlet ground state. The temperature dependence of the magnetic susceptibility of $[Na_9Fe_{20}Se_{38}]^{9-}$, plotted in Figure 8, is consistent with the Mössbauer spectra in showing antiferromagnetic behavior and a singlet ground state.

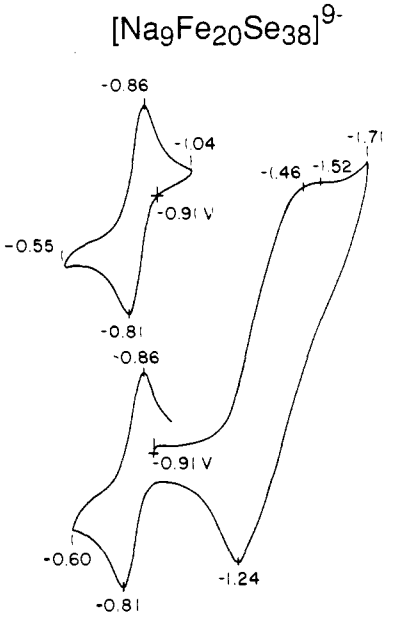

Figure 12. Cyclic voltammograms of $[Na_9Fe_{20}Se_{38}]^{9-}$ in acetonitrile solution (100 mV/s). The lower voltammogram was first scanned to negative potentials. Peak potentials vs SCE are indicated.

The cluster is mixed-valence (18Fe(III) + 2Fe(II)). Subspectra of the ten crystallographically independent iron subsites are unresolved. The spectra were analyzed with a two-subsite model of equal line widths; parameters are contained in Table VI. Nearly all previous Mössbauer data on Fe–Se systems have come from our recent comprehensive study of Fe–Se–SR clusters.[35] The isomer shift of 0.38 mm/s for the majority doublet is comparable with those for $[Fe_2Se_2(SR)_4]^{2-}$ (0.32–0.34 mm/s), indicating an oxidation state near Fe(III). From the empirical relationship between isomer shift and oxidation state for Fe–Se clusters,[35] the shift corresponds to the oxidation state 2.91+. For the minority doublet, we obtain 2.76+, for a weighted mean of 2.86+, which is in good agreement with 2.90+ from the chemical formula. No distinct Fe(II) sites were detected in the spectra. We conclude that this cluster, as $[Fe_4Se_4(SR)_4]^{2-,3-}$ and $[Fe_6Se_9(SR)_2]^{4-}$,[35] is electronically delocalized. The near-identity of the Mössbauer spectra in the solid state and in acetonitrile solution indicates that the bicyclic structure is retained in solution.

(d) Reactivity. As shown by the cyclic voltammograms in Figure 12, $[Na_9Fe_{20}Se_{38}]^{9-}$ undergoes a chemically reversible ($i_{pa}/i_{pc} \approx 1$) oxidation at $E_{1/2} = -0.84$ V. Controlled potential coulometry (30 min) gave $n = 2.05$ F, indicating a two-electron oxidation to an all-Fe(III) cluster. However, the product proved to be insufficiently stable for isolation. The cluster exhibited a quasireversible multi-electron reduction(s) centered near −1.5 V which, from comparison of oxidative and reductive currents, involves 4–6 e^-. However, the cluster evidently was not significantly altered structurally inasmuch as the two-electron process was recovered upon scan reversal.

The reactions of $[Na_9Fe_{20}Se_{38}]^{9-}$ with thiols and thiolates were examined in order to see if new cluster species could be obtained by cleavage of the structure. No reaction was observed between 50 equiv of NaS-*p*-tol (tol = tolyl) and the cluster in Me_2SO solution for 22 h at room temperature followed by heating for 5 h. However, when the cluster was treated with 9.4 equiv of $[Fe(S\text{-}p\text{-}tol)_4]^{2-}$ in acetonitrile solution for 24 h, a black crystalline sparingly soluble product, identified by ^1H NMR spectroscopy as $(Bu_4N)_2[Fe_4Se_4(S\text{-}p\text{-}tol)_4]$,[43] was obtained in quantitative yield based on cation. Workup of the reaction filtrate afforded a small

(38) Q = S: (a) Boon, J. W.; MacGillavry, C. H. *Recl. Trav. Chim. Pays-Bas* **1942**, *61*, 910. (b) Bronger, W. *Z. Anorg. Allg. Chem.* **1968**, *359*, 225. (c) Klepp, K.; Boller, H. *Monatsh. Chem.* **1979**, *110*, 1045. (d) Bronger, W.; Müller, P. *Stud. Inorg. Chem.* **1983**, *3*, 601; *Chem. Abstr.* **1983**, *98*, 226637y. (e) Bronger, W.; Kyas, A.; Müller, P. *J. Solid State Chem.* **1987**, *70*, 262.

(39) There are several exceptions. (a) $Ba_5Fe_4S_{11}$: Steinfink, H. *Adv. Chem. Ser.* **1980**, *186*, 409. (b) $Ba_9Fe_4S_{15}$: Cohen, S.; Rendon-Diazmiron, L. E.; Steinfink, H. *J. Solid State Chem.* **1978**, *25*, 179.

(40) Müller, P.; Bronger, W. *Z. Naturforsch.* **1979**, *34b*, 1264; **1981**, *36b*, 646.

(41) (a) Reiff, W. M.; Grey, I. E.; Fan, A.; Eliezer, Z.; Steinfink, H. *J. Solid State Chem.* **1975**, *13*, 32. (b) Hoggins, J. T.; Steinfink, H. *Acta Crystallogr.* **1977**, *B33*, 673.

(42) (a) Klepp, K.; Boller, H. *Monatsh. Chem.* **1981**, *112*, 83. (b) Boller, H.; Blaha, H. *Monatsh. Chem.* **1983**, *114*, 145.

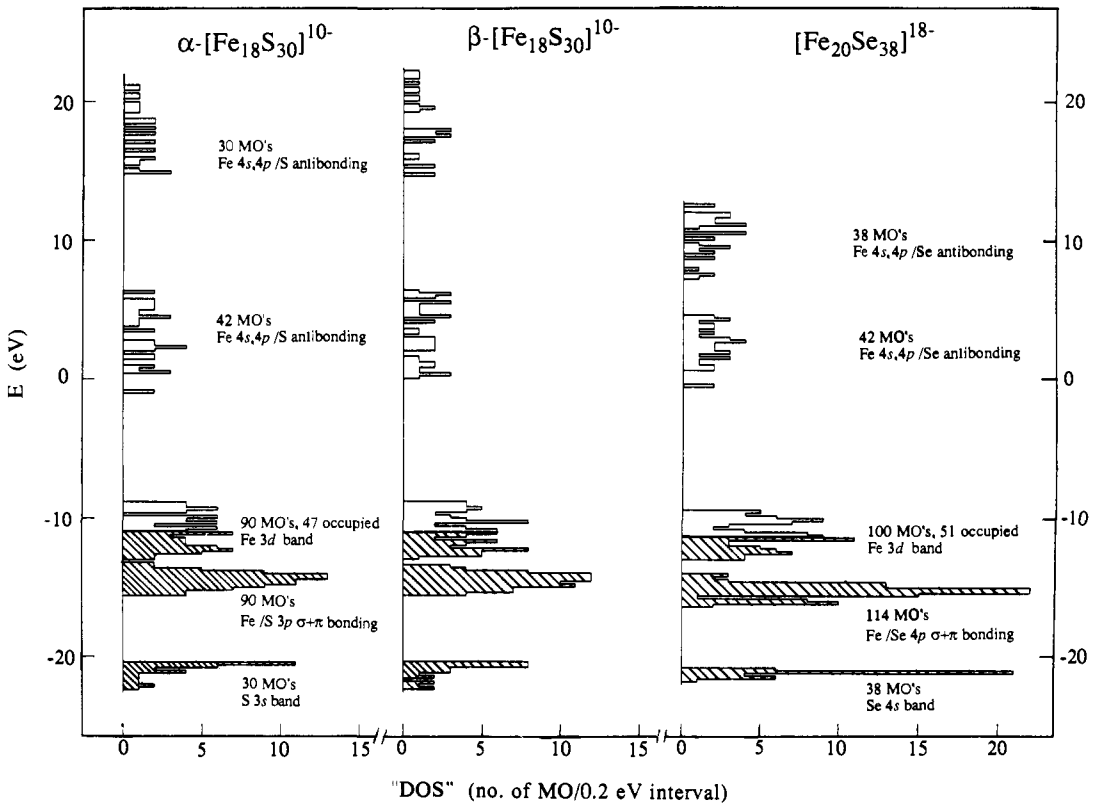

Figure 13. Quasi-density-of-states (DOS) representation of the MO energy level diagrams of α- and β-$[Fe_{18}S_{30}]^{10-}$ and of $[Fe_{20}Se_{38}]^{18-}$ as calculated by the extended Hückel method. The dominant orbital components of each orbital block are indicated; occupied orbitals are shaded.

amount of black solid whose spectroscopic properties indicated it to be the *p*-tol analogue of $[Fe_6Se_9(SEt)_2]^{4-}$.[35,44] Variations in the reaction conditions, including initial mol ratio and reaction time and temperature, afforded mixtures of these two clusters. Treatment of $[Na_9Fe_{20}Se_{38}]^{9-}$ with 60 equiv of *p*-tolSH afforded crystalline $(Bu_4N)_2[Fe_4Se_4(S\text{-}p\text{-}tol)_4]$ in 70% yield based on iron. Similar variations in reaction conditions produced largely the cubane-type cluster as the major product, and the byproducts $[Fe_6Se_9(S\text{-}p\text{-}tol)_2]^{4-}$ and $[Fe_2Se_2(S\text{-}p\text{-}tol)_4]^{2-}$,[45] identified by ^1H NMR spectroscopy. Perhaps the potentially most interesting result, cluster cleavage to afford the chain fragments $[Fe_6Se_{10}(SR)_4]^{6-}$, was not achieved. Among Fe–Q clusters, $[Fe_4S_6(SEt)_4]^{4-}$[37] is the longest linear chain cluster yet isolated. $[Na_9Fe_{20}Se_{38}]^{9-}$ resembles $[\alpha\text{-}Na_2Fe_{18}S_{30}]^{8-}$ in that cleavage reactions with the same reagents afford analogous cluster products.[11] For this reason, the reactions of the β-isomer (other than redox) were not investigated.

Molecular Orbital Description of Electronic Structures. In view of the complexity of the clusters, calculations were performed at the extended Hückel level.[46-48] The two isomers of $[Fe_{18}S_{30}]^{10-}$ and $[Na_4Fe_{18}S_{30}]^{6-}$, and $[Fe_{20}Se_{38}]^{18-}$ and $[Na_{11}Fe_{20}Se_{38}]^{7-}$ with crystallographic C_i and C_2 symmetry, respectively, were examined. The resultant orbital energy spectra of the three Na^+-excluded clusters are presented in Figure 13 as quasi-density-of-states (DOS) diagrams, and in Figure 14 as average Fe–S/Se and Fe–Fe bond overlap populations for individual MO's. The latter plot follows the solid-state notion of COOP (crystal orbital overlap population),[49] which provides an explicit means to determine the principal bonding characteristics of a particular MO. It is immediately evident from these two figures that the three clusters assume quasi-solid-state band structures and exhibit similar band patterns. Thus the 282 MO's of α-$[Fe_{18}S_{30}]^{10-}$ and β-$[Fe_{18}S_{30}]^{10-}$ and the 332 MO's of $[Fe_{20}Se_{38}]^{18-}$ are packed into five blocks or "bands" which, for the most part, are well separated in energy. In referring to properties below, this order of clusters is retained.

In the lowest blocks at ca. −21 eV are the most stable orbitals, which are of dominant S 3s or Se 4s character and weak Fe–S/Se bonding effects, and equal the number of chalcogenide (Q) atoms in the clusters. The next bands at ca. −15 eV consist of 90 or 114 levels (3× the number of Q atoms) in closely packed intervals (2.17, 1.72, 2.21 eV). From Figure 14, the lower orbitals contribute most strongly to Fe–Q $\sigma + \pi$ bonding while the large majority in the upper half are essentially Fe–Fe nonbonding. Above this block and centered at ca. −11 eV are the Fe 3d bands consisting of 90 or 100 MO's (5× the number of Fe atoms) over the intervals 4.13, 4.00, and 3.45 eV. These contain the HOMO's and LUMO's with the slight apparent energy separations indicated in Figure 13. Above these bands are the fourth and fifth orbital blocks with the indicated antibonding characteristics.

In the Fe 3d block, the lower one-third is dominated by Fe–Fe bonding together with nonbonding and weakly antibonding Fe–Q interactions. Consistent with the singlet ground states of α- and β-$[Fe_{18}S_{30}]^{10-}$, 47 d-type MO's are occupied; their character may be specified further. There are 24 (α) and 22 (β) MO's that are Fe–Fe bonding, equal to the number of Fe–Fe bonding connections between adjacent atoms in the clusters. Among the remaining MO's, five (α) and seven (β) are Fe–Fe nonbonding or weakly Fe–Q antibonding, and 18 in both clusters are Fe–Fe and Fe–S antibonding, thereby roughly cancelling the effects of 18 such

(43) Reynolds, J. G.; Coyle, C. L.; Holm, R. H. *J. Am. Chem. Soc.* **1980**, *102*, 4350.

(44) $[Fe_6Se_9(p\text{-}tol)_2]^{4-}$ in MeCN: λ_{max} 302, 305 (sh), 460, 590 (sh); ^1H NMR, δ 4.80, 5.18 (br), 8.54. $[Fe_6Se_9(SPh)_2]^{4-}$ in MeCN:[35] λ_{max} 327, 440 (sh), 588 (sh) nm. $[Fe_6S_9(SPh)_2]^{4-}$ in Me_2SO: λ_{max} 300, 350 (sh), 420 (sh), 530 (sh); ^1H NMR, δ 4.87, 5.7 (br), 8.27 (Christou, G.; Sabat, M.; Ibers, J. A.; Holm, R. H. *Inorg. Chem.* **1982**, *21*, 3518).

(45) Reynolds, J. G.; Holm, R. H. *Inorg. Chem.* **1980**, *19*, 3257.

(46) Fe and S parameters: Silvestre, J.; Hoffmann, R. *Inorg. Chem.* **1985**, *24*, 4108.

(47) Se parameters: Hughbanks, T.; Hoffmann, R. *J. Am. Chem. Soc.* **1983**, *105*, 1150.

(48) Na parameters: Burdett, J. K. *Molecular Shapes*; Wiley: New York, 1980; Chapter 2.

(49) Hoffmann, R. *Solids and Surfaces*; VCH Publishers: New York, 1988; pp 43ff, and references therein.

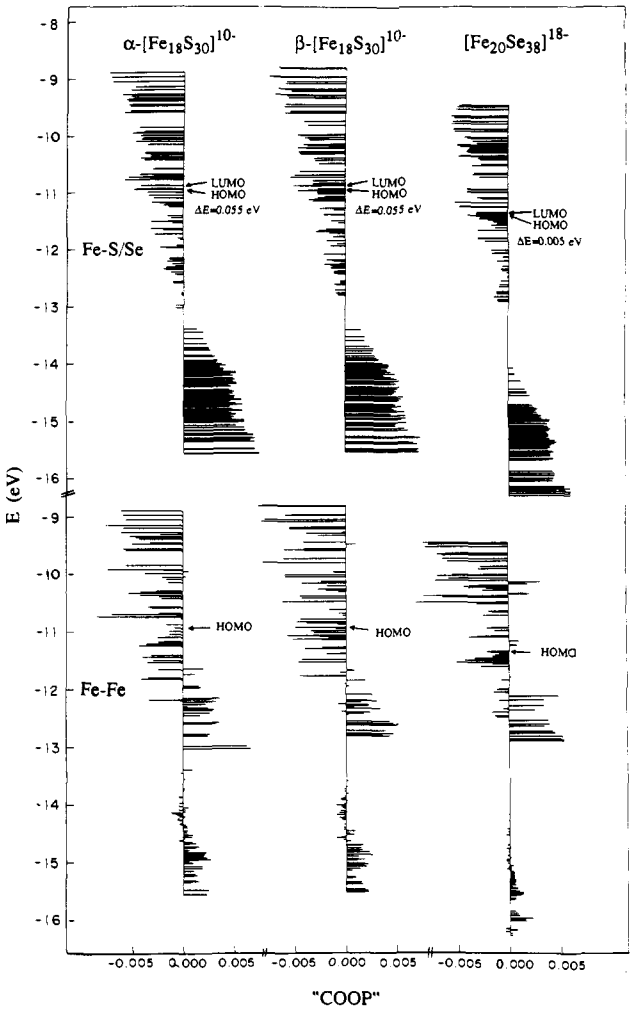

Figure 14. Average overlap population for each MO for Fe–S/Se (upper) and Fe–Fe (lower) bonding interactions in α- and β-$[Fe_{18}S_{30}]^{10-}$ and $[Fe_{20}Se_{38}]^{18-}$. Positive values imply bonding interactions and negative values antibonding interactions.

MO's in the 90-orbital Fe–S bonding group. This reduces to 72 the number of effective Fe–S interactions, which is 4× the number of μ_4-S atoms, 3× the number of μ_3-S atoms, and 2× the number of μ_2 atoms. A less strict correlation of molecular topology with the MO bonding scheme also holds for $[Fe_{20}Se_{38}]^{18-}$. Of the 51 filled d-type MO's, 19 are Fe–Fe bonding and 2 are weakly bonding in this sense, as compared to the 21 Fe–Fe bonding connections in the cluster. Apart from the 19 Fe–Fe MO's, the remaining 32 orbitals are Fe–Se antibonding (3 weakly so). This is two short of the 34 MO's that would have been required to reduce the contributions of 114 bonding orbitals in the Fe–Se bonding block to 80, the number of Fe–Se bonding connections. Perhaps Fe–Se bonding has been increased in order to compensate for the lost Fe–Fe bonding effects owing to the elevation of several Fe–Fe bonding orbitals to the unfilled region (Figure 14).

The following are the principal conclusions from the MO calculations: (i) Compositions of filled MO's imply extensive electron delocalization. (ii) The HOMO's and LUMO's are Fe–Q and Fe–Fe antibonding (weakly so in several cases). (iii) The small HOMO–LUMO energy gaps are consistent with the thermal population of paramagnetic states observed in the magnetic susceptibilities. (iv) Inclusion of four and eleven sodium ions in the calculations of Fe_{18} and Fe_{20} clusters, respectively, has only a minor effect on the relative energy level schemes and on Fe–Fe and Fe–Q interactions. However, some general trends were found. The Fe–Q bonding bands are widened and stabilized, Fe–Q bonding overlap populations are improved, the antibonding effects in the unoccupied d-type MO's are reduced, apparent charges on Q atoms that interact with Na^+ are lowered, and the energy

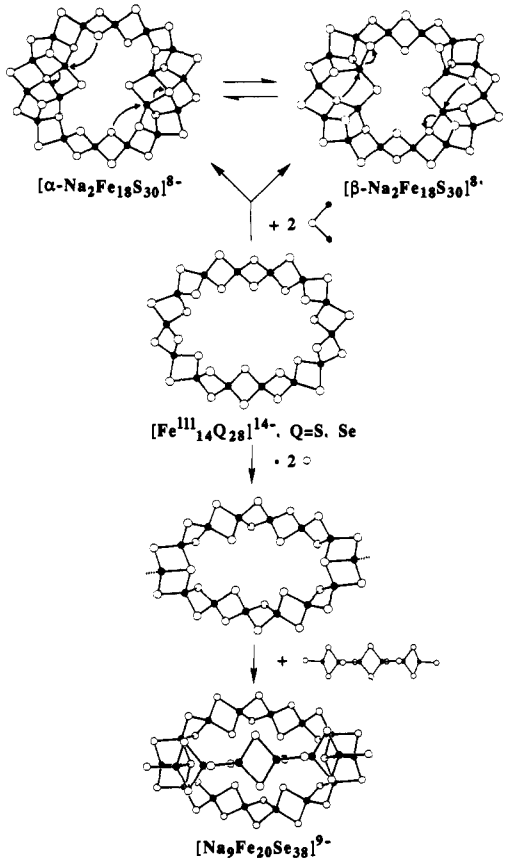

Figure 15. Illustration of the conceptual construction of the clusters $[\alpha\text{-}Na_2Fe_{18}S_{30}]^{8-}$, $[\beta\text{-}Na_2Fe_{18}S_{30}]^{8-}$, and $[Na_9Fe_{20}Se_{38}]^{9-}$ from a common precursor ring $[Fe_{14}Q_{28}]^{14-}$ (Q = S, Se) and of the conceptual interconversion of the α- and β-isomers. The $Fe_{14}Q_{28}$ fragment is retained as a perimeter ring in the final cluster structures. Sodium ions, which stabilize all structures shown, are omitted.

differences between the sodium-containing and sodium-free Fe_{18} and Fe_{20} clusters are 5 and 15 eV, respectively. (v) The average of the net charges of the four nonperimeter Fe atoms in α- and β-$[Na_4Fe_{18}S_{30}]^{10-}$ (Fe(4,4′,7,7′) in α, Fe(4,4′,8,8′) in β) is significantly less than those of the perimeter Fe_{14} atoms, suggesting (as from structural considerations) that these are the ferrous-like sites whose presence is indicated by Mössbauer spectroscopy. For $[Na_{11}Fe_{20}Se_{38}]^{7-}$, the net charges of the two bridgehead anchor atoms Fe(10,10′) are substantially higher than the average of the net charges of the remaining Fe atoms. (vi) The net charges of the S or Se atoms decrease with increasing bridge multiplicity and overlap populations follow the order Fe–(μ_2-S) > Fe–(μ_3-S) > Fe–(μ_4-S), consistent with Fe–S bond distances. (vii) The two isomers of the Fe_{18} cluster show highly similar bonding schemes and differ in energy by only 0.35 eV. This is indicative of decreased dependence of overall electronic structure on molecular structural details of isomers when cluster nuclearity is sufficiently high.

Cluster Structural Relationships. Topological analysis of the $[Fe_{18}Q_{30}]^{z-}$ case with eqs 1 and 2 affords seven solutions $[n_{\mu 2},n_{\mu 3},n_{\mu 4}]$.[50] Two of these, [18,12,0] and [20,8,2], are manifested as $[\beta\text{-}Na_2Fe_{18}S_{30}]^{8-}$ and $[\alpha\text{-}Na_2Fe_{18}S_{30}]^{8-}$, respectively. There are three solutions for the $[Fe_{20}Q_{38}]^{z-}$ problem;[50] [36,0,2] is represented by $[Na_9Fe_{20}Se_{38}]^{9-}$. As different as these experimentally realized topologies may appear to be, they contain a common structural fragment, viz, a closed $[Fe_{14}Q_{28}]^{z-}$ perimeter ring formed from vertex-sharing of 14 Fe_2Q_2 rhombs. This ring may be visualized as containing inner and outer Q_{14} rings between

(50) $[Fe_{18}Q_{30}]^{z-}$: $[n_{\mu 2},n_{\mu 3},n_{\mu 4}]$ = [18,12,0], [19,10,1], [20,8,2], [21,6,3], [22,4,4], [23,2,5], [24,0,6]. $[Fe_{20}Q_{38}]^{z-}$: $[n_{\mu 2},n_{\mu 3},n_{\mu 4}]$ = [34,4,0], [35,2,1], [36,0,2].

which is a Fe_{14} ring. As shown in Figure 15, the three clusters can be formally constructed from this cyclic fragment. Addition of two $Fe_2(\mu_2\text{-}S)$ fragments gives rise to the two isomers of $[Na_2Fe_{18}S_{30}]^{8-}$. When the two Fe atoms each bind *five* consecutive S atoms of the inner S_{14} ring in the bridging modes $4\mu_3\text{-}S + \mu_4\text{-}S$, the α-isomer is produced. When the binding interactions encompass *six* consecutive S atoms and the modes $6\mu_3\text{-}S$, the β-isomer is generated. The two isomers can be interconverted by the indicated intramolecular sulfide atom attacks on the electrophilic iron centers with consequent topological rearrangement. From isolated yield data based on iron (Figure 3), we infer, but cannot prove, that two isomers exist in equilibrium in alcoholic solution, possibly also with $[FeS_2]_n^{n-}$, and that the equilibrium is shifted by selective precipitation of one isomer as dependent on solvent and cation.

In a similar manner, the expulsion of two Se anions at diagonally opposite ends of the ring generates two edge-shared Fe_2Se_2 rhombs and two three-coordinate iron sites. Addition of a $Fe_6(\mu_2\text{-}Se)_{10}Se_2$ chain fragment and formation of one Fe–$(\mu_2$-Se) and one Fe–$(\mu_4$-Se) bond at each end of the ring builds the three edge-fused bridgehead rhombs and recovers the bicyclic structure of $[Na_9Fe_{20}Se_{38}]^{9-}$.

While the foregoing manipulations are purely conceptual and may not resemble the true assembly mechanisms of the clusters, they do point to a common precursor, $[Fe^{III}{}_{14}Q_{28}]^{14-}$, stabilized by sodium ions. This species is in turn derivable by cyclization of the polymer $[FeQ_2]_n^{n-}$, known in linear form in solid-state compounds.[38de] We prefer an all-Fe(III) formulation of the precursor because, as noted, vertex-shared Fe_2Q_2 rhombs nearly always occur in the Fe(III) state. We observe that, collectively, $[\alpha\text{-}Na_2Fe_{18}S_{30}]^{8-}$, $[\beta\text{-}Na_2Fe_{18}S_{30}]^{8-}$, and $[Na_9Fe_{20}Se_{38}]^{9-}$ contain the majority of Fe_xQ_y cores known in molecular Fe–Q clusters. These include linear Fe_2Q_2, linear and cuboidal Fe_3Q_4, linear Fe_4Q_6, and Fe_6Q_9. We note that $[\beta\text{-}Na_2Fe_{18}S_{30}]^{8-}$ is the first synthetic molecular cluster to contain cuboidal Fe_3Q_4 *not* as part of Fe_6Q_9. A similar cuboidal Fe_3Se_4 unit with three terminal selenide bridges occurs in the phase $Ba_3Fe_3Se_7$ prepared at high temperatures.[51] Lastly, there is perhaps no better example of the apparent assembly of clusters from recognized fragments than that provided by this set of three nanometer-sized clusters, which includes a unique example of cluster isomerism. Given the possibilities provided by the topological analysis, it appears that an extensive family of chalcogenometalates should exist based on metals with a tetrahedral stereochemical preference. The cluster set $[\alpha\text{-}Na_2Fe_{18}S_{30}]^{8-}$, $[\beta\text{-}Na_2Fe_{18}S_{30}]^{8-}$, and $[Na_9Fe_{20}Se_{38}]^{9-}$ demonstrates the (conceptual) principle that in the presence of an appropriate promotor (here Na(PhNCOMe)) high-nuclearity clusters can be assembled by the termination of a unidimensional polymeric fragment via mono- or bicyclization. This approach may lead to the discovery of new regimes of nanometer-sized clusters.

Acknowledgment. This research was supported at Harvard University by NIH Grant GM 28856 and at M.I.T. by ONR Grant NO0014-89-J-1779. X-ray diffraction equipment was obtained by NIH Grant 1 S10 RR 02247. We thank Dr. B. S. Snyder for experimental assistance in the eariy stages of this work.

Supplementary Material Available: Listing of X-ray crystallographic data for the compounds in Table I and tables of intensity collections, atom positional and thermal parameters, and calculated hydrogen atom positions (17 pp); listing of calculated and observed structure factors (143 pp). Ordering information is given on any current masthead page.

(51) Hong, H. Y.; Steinfink, H. *J. Solid State Chem.* **1972**, *5*, 93.

Communications to the Editor

On the Nature of the Olefination Reaction Involving Ditungsten Hexaalkoxides and Aldehydes or Ketones

M. H. Chisholm,* J. C. Huffman, E. A. Lucas, A. Sousa, and W. E. Streib

Department of Chemistry and Molecular Structure Center Indiana University Bloomington, Indiana 47405

Received September 3, 1991
Revised Manuscript Received January 22, 1992

Pertinent to the development of any reagent for organic synthesis is a knowledge of its scope, limitations, reaction mechanism, and competing side reactions. We are investigating the use of ditungsten hexaalkoxides for the reductive coupling of aldehydes and ketones to olefins.[1] This reaction proceeds in two stages: (1) the reductive cleavage of the carbonyl group of the aldehyde or ketone to yield a μ-alkylidene oxo ditungsten compound (eq 1)[2] and (2) formation of the olefinic C–C bond and rupture of the carbonyl C–O bond of the second aldehyde or ketone. We report here observations that provide insight into the nature of the initial C–O bond cleavage and subsequent C–C bond formation.

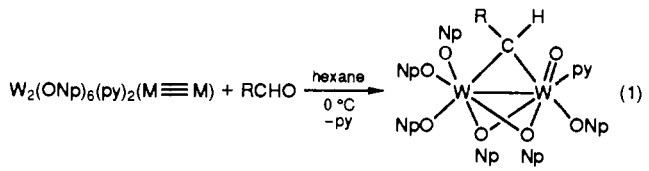

(1)

The addition of cyclopropanecarboxaldehyde (1 equiv) to $W_2(ONp)_6(py)_2$, where Np = neopentyl and py = pyridine, in hexane at 0 °C gives the cyclopropylmethylidene complex $W_2(ONp)_6(\mu\text{-}CH(C_3H_5))(O)(py)$ as dark red crystals in ca. 70% yield.[3] The structure of this complex is shown in Figure 1[4] and resembles the previously characterized related complexes $W_2(ONp)_6(\mu\text{-}CHAr)(O)(py)$.[5] To our knowledge, this is the first structurally characterized cyclopropylmethylidene complex,[6] and

(1) Chisholm, M. H.; Klang, J. A. *J. Am. Chem. Soc.* **1989**, *111*, 2324.
(2) For examples of C=O cleavage by mononuclear W^{II} compounds and mechanistic studies thereof, see: Bryan, J. C.; Mayer, J. M. *J. Am. Chem. Soc.* **1990**, *112*, 2298.

(3) All reactions were carried out under dry and oxygen-free atmospheres (N_2) and employed purified, deoxygenated solvents. Satisfactory elemental analyses were obtained.
(4) Crystal data for $W_2(O)(OCH_2\text{-}t\text{-}Bu)_6(\mu\text{-}C_4H_6)(py)$ at −170 °C: a = 12.606 (2) Å, b = 19.923 (4) Å, c = 10.583 (2) Å, α = 104.52 (1)°, β = 112.21 (1)°, γ = 95.16 (1)°, Z = 2, d_{calcd} = 1.48 g cm^{-3}, and space group $P\bar{1}$. For $W_2(O)(OCH_2\text{-}t\text{-}Bu)_6(\mu\text{-}OC_{12}H_{16})$ at −169 °C: a = 11.227 (2) Å, b = 20.634 (3) Å, c = 10.730 (2) Å, α = 104.73 (1)°, β = 98.31 (1)°, γ = 75.56 (1)°, Z = 2, d_{calcd} = 1.55 g cm^{-1}, and space group $P\bar{1}$.
(5) Chisholm, M. H.; Lucas, E. A.; Sousa, A. C.; Huffman, J. C. *J. Chem. Soc., Chem. Commun.* **1991**, 847.
(6) (a) Brookhart, M.; Studabaker, W. B.; Husk, G. R. *Organometallics* **1985**, *4*, 943. (b) One (trinuclear) cyclopropylmethylidyne complex has been structurally characterized. See: Seidler, P. F.; McKenna, S. T.; Kulzick, M. A.; Gilbert, T. M. *Acta Crystallogr.* **1985**, *C41*, 352.

0002-7863/92/1514-2710$03.00/0